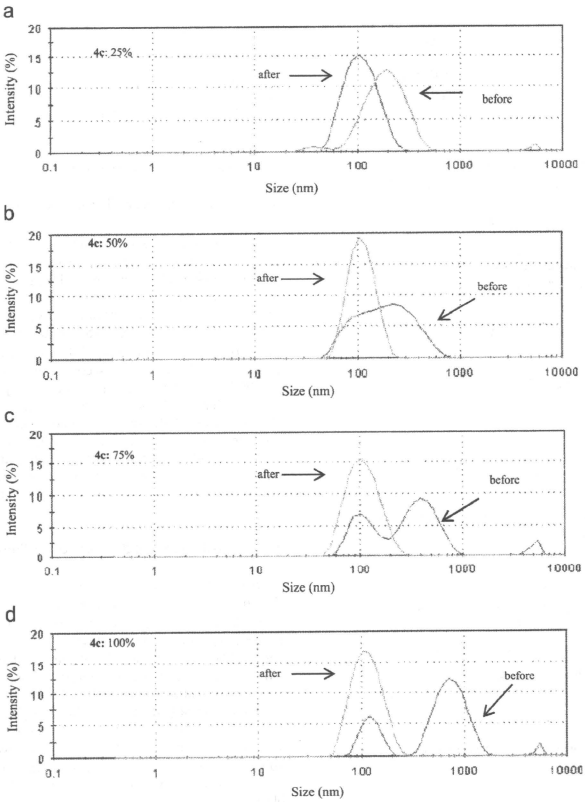

Fig. 3. Size distributions of the boron liposomes prepared from cholesterol, DSPC, PEG-DSPE, and **4c** (1/1-X/0.1/X; (a) $X = 0.25$, (b) $X = 0.5$, (c) $X = 0.75$, (d) $X = 1$) before- and after-extrusion.

after neutron irradiation, boron liposomes have a potential for effective boron delivery vehicle on BNCT.

Acknowledgment

This work was supported by The New Energy and Industrial Technology Development Organization (NEDO) research project of developing a hospital based accelerator for boron neutron capture therapy with advanced drug delivery system.

References

Barth, R.F., Coderre, J.A., Vicente, M.G.H., Blue, T.E., 2005. Boron neutron capture therapy of cancer: current status and future prospects. Clin. Cancer. Res. 11 (11), 3987.

Feakes, D.A., Shelly, K., Knobler, C.B., Hawthorne, M.F., 1994. $Na_3[B_{20}H_{17}NH_3]$: synthesis and liposomal delivery to murine tumors. Proc. Natl. Acad. Sci. USA 91, 3029–3033.

Feakes, D.A., Shelly, K., Hawthorne, M.F., 1995. Selective boron delivery to murine tumors by lipophilic species incorporated in the membranes of unilamellar liposomes. Proc. Natl. Acad. Sci. USA 92, 1367–1370.

Gabel, R., Moller, D., Harfst, S., Rosler, J., Ketz, H., 1993. Synthesis of S-alkyl and S-acyl derivatives of mercaptoundecahydrododecaborate, a possible boron carrier for neutron capture therapy. Inorg. Chem. 32, 2276–2278.

Justus, E., Awad, D., Hohnholt, M., Schaffran, T., Edwards, K., Karlsson, G., Damian, L., Gabel, D., 2007. Synthesis, liposomal preparation, and in vitro toxicity of two novel dodecaborate cluster lipids for boron neutron capture therapy. Bioconjugate Chem. 18, 1287–1293.

Kullberg, E.B., Carlsson, J., Edwards, K., Capala, J., Sjöberg, S., Gedda, L., 2003. Introductory experiments on ligand liposomes as delivery agents for boron neutron capture therapy. Int. J. Oncol. 23, 461–467.

Lee, J.D., Ueno, M., Miyajima, Y., Nakamura, H., 2007. Synthesis of boron cluster lipids: closo-dodecaborate as an alternative hydrophilic function of boronated liposomes for neutron capture therapy. Org. Lett. 9, 323–326.

Li, T., Hamdi, J., Hawthorne, M.F., 2006. Unilamellar liposomes with enhanced boron content. Bioconjugate Chem. 17, 15–20.

Locher, G.L., 1936. Biological effects and therapeutical possibilities of neutrons. Am. J. Roentgenol. Radium Ther. 36, 1–13.

Maruyama, K., Ishida, O., Kasaoka, S., Takizawa, T., Utoguchi, N., Shinohara, A., Chiba, M., Kobayashi, H., Eriguchi, M., Yanagie, H., 2004. Intracellular targeting of sodium mercaptoundeca-hydrododecaborate (BSH) to solid tumors by

transferrin-PEG liposomes, for boron neutron-capture therapy (BNCT). J. Control. Release 98, 195–207.
Miyajima, Y., Nakamura, H., Kuwata, Y., Lee, J.D., Masunaga, S., Ono, K., Maruyama, K., 2006. Transferrin-loaded nido-carborane liposomes: tumor-targeting boron delivery system for neutron capture therapy. Bioconjugate Chem. 17, 1314–1320.
Nakamura, H., Miyajima, Y., Takei, T., Kasaoka, T., Maruyama, K., 2004. Synthesis and vesicle formation of a nido-carborane cluster lipid for boron neutron capture therapy. Chem. Commun., 1910–1911.
Pan, X.Q., Wang, H., Shukla, S., Sekido, M., Adams, D.M., Tjarks, W., Barth, R.F., Lee, R.J., 2002. Boron-containing folate receptor-targeted liposomes as potential delivery agents for neutron capture therapy. Bioconjugate Chem. 13, 435–442.
Pan, X., Wu, G., Yang, W., Barth, R.F., Tjarks, W., Lee, R.J., 2007. Synthesis of cetuximab-immunoliposomes via a cholesterol-based membrane anchor for targeting of EGFR. Bioconjugate Chem. 18, 101–108.
Shelly, K., Feakes, D.A., Hawthorne, M.F., Schmidt, P.G., Krisch, T.A., Bauer, W.F., 1992. Model studies directed toward the boron neutron-capture therapy of cancer: boron delivery to murine tumors with liposomes. Proc. Natl. Acad. Sci. USA 89, 9039–9043.
Yanagie, H., Tomita, T., Kobayashi, H., Fujii, Y., Takahashi, T., Hasumi, K., Nariuchi, H., Sekiguchi, M., 1991. Application of boronated anti-CEA immunoliposome to tumor cell growth inhibition in in vitro boron neutron capture therapy model. Br. J. Cancer 63, 522–526.

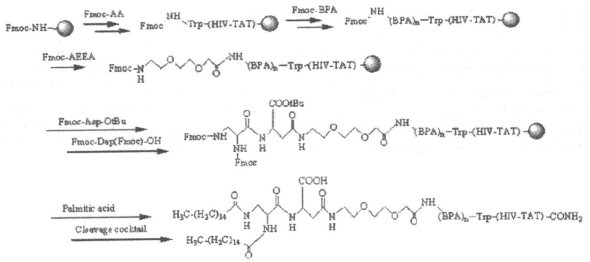

Fig. 1. Synthesis of the HIV-TAT and BPA peptide conjugated lipid analog.

Table 1
Composition of B5-TAT-lpopeptide modified liposome.

	DSPC	Cholesterol	DSPE-PEG2000	Bn-TAT-peptide
Plain liposome	50	50	–	–
PEG-liposome	47	47	6	–
B5-TAT5% PEG-liposome	45	45	5	5
B5-TAT10% PEG-liposome	42.5	42.5	5	10

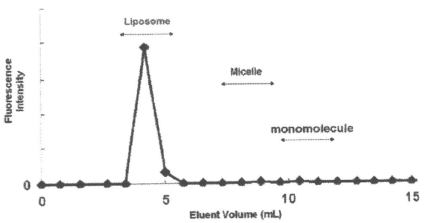

Fig. 2. Gel filtration chromatography of liposome, micelle, and monomolecule.

through polycarbonate membrane using an extruder, yielding the peptide-modified liposome (Table 1).

2.3. Gel filtration chromatography

The prepared liposome was subjected to size exclusion chromatography, which separated the liposome, micelle and monomolecule fractions, and the content of the lipopeptide was determined (Fig. 2). The liposome was then measured using the fluorescence of the tryptophan residue of the lipopeptide.

3. Results

3.1. Identification of lipopeptide

In the case of $n = 5$ (B5-TAT), the C8-column used for high performance liquid chromatography (HPLC) analysis showed the main peak (retention time at 13.6 min) accompanied by the existence of some impurities (Fig. 3a). However, the synthesis of conjugated lipopeptide attached to palmitoyl chain as an anchor

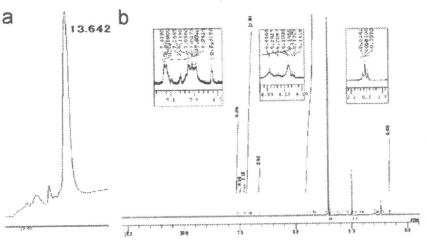

Fig. 3. Identification of HIV-TAT peptide and BPA conjugated lipid analog B5-TAT. (a) C8-HPLC, (b) ^{1}H NMR.

domain proceeded very smoothly. HPLC analysis showed almost one peak, and ESI-TOFMS (electrospray ionization mass spectroscopy) showed m/z 3504 of the dehydration peak as an exact mass of m/z 3522. In addition, ^{1}H NMR analysis (JEOL JMN-AL400) also showed the structure of the lipopeptide; for example, the molar ratio of the TAT-peptide and palmitoyl moiety showed the correct proton ratio of the ortho position on the tyrosine residue (2H as a characteristic signal of the peptide at 6.62 ppm) to the methyl signal at 0.81 ppm in the alkyl chain end (6H as a characteristic signal of the lipid) using an integration value of ^{1}H NMR spectra (Fig. 3b). The overall yield of the lipopeptide was greater than 70% based on the molar ratio of the amino group on TGS-RAM resin.

3.2. Incorporated ratio of lipopeptide

The incorporation of lipopeptide into the liposome was examined. Synthesized lipopeptide was incorporated into the liposome effectively. The incorporated ratios of lipopeptide to liposome are summarized in Table 2.

3.3. Physical properties of liposomes

We examined the diameter of the liposomes with monodispersion and zeta-potential by means of dynamic light scattering measurement (Zetasizer Nano ZS, Malvern Instruments Ltd.) liposomes, which were composed of DSPC, cholesterol, DSPE-PEG, and the lipopeptide were prepared by the lipid-film method followed by extrusion. The diameters of the liposomes were

Table 2
Liposome formation and lipopeptide incorporated into liposome.

Lipopeptide	Theoretical lipopeptide ratio (mol%)	Incorporated ratio (%)
B5-TAT lipopeptide	5	66.1
	10	73.4

Table 3
Physicochemical property of functionalized liposome.

DSPC/Chol/DSPE-PEG/B-TAT (molar ratio)		Particle size (nm, u/G2)	Zeta potential (mV)
Plain liposome	50/50/0/0	147	−40
PEG-liposome	47/47/6/0	143	−15
B3-TAT lipopeptide liposome	45/45/5/5	120.3	17.5
	42.5/42.5/5/10	101.3	20.7
B5-TAT lipopeptide liposome	45/45/5/5	105.9	21
	42.5/42.5/5/10	147.8	26.4

shown to be about 100 nm. The positive charge of the peptide-modified liposome indicated the presence of basic peptide HIV-TAT on the liposome surface. The characteristics of liposomal formulations containing BPA conjugate peptide are summarized in Table 3.

4. Discussion

We synthesized a new peptide lipid containing multiple BPA components and a TAT domain for use in a boron-containing liposome which can encapsulate a boron compound in its internal water phase. The peptide lipid can be efficiently incorporated into liposomes that are 100 nm in diameter.

HIV-TAT was first developed from reverse transcriptase of HIV. It is a kind of protein transduction domain (Green and Loewenstein, 1998) which can introduce intracellular protein, deoxyribonucleic acid and macromolecular-containing liposome (Wadia et al., 2004; Eric and Steven, 2004; Fretz et al., 2005). Yagi et al. reported an in vitro anti-tumor effect of DOX encapsulated by TAT-modified liposome in 2007 (Yagi et al., 2007). The TAT-conjugating liposome facilitated an in vitro gene expression as well as in vivo expression when the same liposome was locally injected (Torchilin et al., 2003).

Active targeting against tumor cells using TAT have been evaluated; however, there is no previous report involving a boron-containing TAT liposome or compound.

A sufficient concentration of boron is necessary for successful BNCT. Thus, a material with high boron content generally has an advantage (Maruyama et al., 2004). Nakamura et al. developed a double-stranded boron cluster in 2004 (Lee et al., 2007). In the present study, the peptide lipid synthesized contains only 1–5 boron in a single molecule. However, our peptide lipid allows the number of boron to be increased up to $n = 12$ or 15.

In general, the hydrophilic charge of BSH in a boron-containing liposome has certain difficulty in encapsulating more BSH in the internal water phase of the liposome itself. There has been no previous report involving encapsulated BSH in the internal water phase within a boron liposome. Our peptide modification liposome of the hydrophilic charge is aspartic acid, and it shows high performance in terms of film stability and has a potential advantage in encapsulating BSH in the liposome in which the lipopeptide conjugate BPA.

Further investigation is needed to determine the in vitro and in vivo toxicity and the boron introduction efficiency.

5. Conclusions

We succeeded in synthesizing a lipopeptide containing boron. This lipopeptide could be incorporated into the liposome effectively. After toxicity testing, these liposomes will be administered to the cells or in vivo as a new BDS candidate.

Acknowledgments

This study was supported in part by a grant-in aid from the Ministry of Health, Labour and Welfare (WGA22039).

References

Barth, R.F., Coderre, J.A., Vicente, M.G., Blue, T.E., 2005. Clin. Cancer Res., 3987–4002.
Eric, L.S., Steven, F.D., 2004. Pharm. Res. 21 (3), 389–393.
Fretz, M.M., Mastrobattista, E., Koning, G.A., Jiskoot, W., Storm, G., 2005. Int. J. Pharm. 298 (2), 305–309.
Green, M., Loewenstein, P.M., 1998. Cell 55 (6), 1179–1888.
Lee, J.-D., Ueno, M., Miyajima, Y., Nakamura, H., 2007. Org. Lett. 9, 323–326.
Locher, G.L., 1936. Am. J. Roentgenol. 36, 1–13.
Maruyama, K., Ishida, O., Kasaoka, S., Takizawa, T., Utoguchi, N., Shinohara, A., Chiba, M., Kobayashi, H., Eriguchi, 2004. J. Controlled Release 98, 195–207.
Nakamura, H., 2008. Yakugaku zasshi 128 (2), 193–208.
Solid-phase Synthesis Handbook. Merk.
Soloway, A.H., Tjarks, W., Barnum, B.A., Rong, F-G., Barth, R.F., Codogni, I.M., Wilson, J.G., 1998. Chem. Rev. 98, 1515–1562.
Torchilin, V.P., Levchenko, T.S., Rammohan, R., Volodina, N., Papahadjopoulos-Sternberg, B., D'Souza, G.G.M., 2003. Proc. Natl. Acad. Sci. USA 100 (4), 1972–1977.
Vives, E., 2003. J. Mol. Recognit. 16, 265–271.
Wadia, J.S., Stan, R.V., Dowdy, S.F., 2004. Nat. Med. 10 (3), 310–315.
Yagi, N., Ogawa, Y., Kodaka, M., Okada, T., Tomohiro, T., Konakahara, T., Okuno, H., 2000. Lipids 20, 673–679.
Yagi, N., Yano, Y., Hatanaka, K., Yokoyama, Y., Okuno, H., 2007. Biomed. Lett. 17, 2590–2593.

Applied Radiation and Isotopes 67 (2009) S88–S90

Contents lists available at ScienceDirect

Applied Radiation and Isotopes

journal homepage: www.elsevier.com/locate/apradiso

Synthesis and evaluation of a novel liposome containing BPA–peptide conjugate for BNCT

Makoto Shirakawa [a,*], Tetsuya Yamamto [a], Kei Nakai [a], Kenichi Aburai [b], Sho Kawatobi [c], Takao Tsurubuchi [a], Yohei Yamamoto [a], Yuusaku Yokoyama [c], Hiroaki Okuno [c], Akira Matsumura [a]

[a] Department of Graduate School of Comprehensive Human Sciences, Faculty of Functional and Regulatory Medical Sciences, University of Tsukuba, Japan
[b] Department of Pure and Applied Chemistry, Faculty of Science and Technology, Tokyo University of Science, Japan
[c] Faculty of Pharmaceutical Sciences, Toho University, Japan

ARTICLE INFO

Keywords:
Boron neutron capture therapy (BNCT)
Boron delivery system (BDS)
Liposome
Boronophenylalanine (BPA)
HIV-TAT

ABSTRACT

We aimed at securing sufficient concentrations of ^{10}B in boron neutron capture therapy (BNCT) by developing a new drug delivery system. We have designed and developed a novel lipid analog and succeeded in using it to develop the new boron component liposome. It consisted of three different kinds of amino acid derivatives and two fatty acids, and could react directly with the peptide synthesized first on resin by Fmoc solid-phase synthesis. In this study, lipid analog conjugated with HIV-TAT peptide (domain of human immunodeficiency virus TAT protein) and boronophenylalanine (BPA) was synthesized and successfully incorporated into liposomes.

1. Introduction

Boron neutron capture therapy (BNCT) is a tumor-selective radiation modality which depends on a sufficient cellular uptake of boron (^{10}B) followed by irradiation with a beam of thermal or epithermal neutrons (Barth et al., 2005; Soloway et al., 1998; Locher, 1936). ^{4}He and ^{7}Li particles are produced during the neutron capture reaction and damage DNA, which leads to cell killing. Regarding BNCT, the short radiation range of ^{4}He and ^{7}Li particles is decisive for the distribution of ^{10}B. Thus, successful treatment of cancer by BNCT requires the selective delivery of relatively large amounts of ^{10}B compound to malignant cells. The estimated boron concentration required for effective therapy is in the range of 20–30 μg ^{10}B per g tissue (Nakamura, 2008). However, there have been no ideal boron compounds that fulfill the conditions of low toxicity, water solubility, and low distribution in normal tissue. Therefore, we aimed at securing sufficient concentrations of ^{10}B in BNCT by developing a new drug delivery system.

2. Materials and methods

2.1. Synthesis of lipopeptide

Lipopeptide conjugated with HIV-TAT (Vives, 2003) peptide and boronophenylalanine (BPA) was synthesized on TGS-RAM resin by the Fmoc solid-phase synthesis method (Solid-phase Synthesis Handbook) using an automatic peptide synthesizer (Shimadzu PSSM-8 Peptide Synthesizer Simultaneous Multiple) (Yagi et al., 2000) (Fig. 1). Tryptophan residue was added at the N-terminus of HIV-TAT peptide as a fluorescence probe. BPA was coupled arbitrarily. Then, Fmoc-AEEA (9-fluorenylmethoxycarbonyl-8-amino-3,6-dioxaoctanoic acid, linker domain), Fmoc-Asp-OtBu (hydrophilic domain), and Fmoc-Dap (Fmoc)–OH (glycero mimic domain) were coupled sequentially. Benzotriazole-1-yl-oxy-tris-pyrrolidino-phosphonium hexafluorophosphate (PyBOP), N-hydroxybenzotriazole (HOBt), and N-methyl morpholine (NMM) were used, respectively, for the peptide coupling reaction with 1.0, 1.0, and 1.5 equivalents based on amino acids. Fmoc amino acid and alkyl chain were used for resin in an equivalent of the excess of 7 and 6, respectively. Each coupling reaction was carried out for 30 min. The last condensation reaction with palmitic acid was carried out in a manual mode with the reaction progress checked by a ninhydrin test. De-protection and cleavage of resin were accomplished with a cleavage cocktail (10 mg/mL of 2-methylindole containing trifluoroacetic acid /H_2O/thioanisole/1,2-ethanedithiol/ethylmethyl sulfide/phenol = 82/5/5/3/2/3) for 16 h at room temperature, then precipitated by adding a large amount of diethyl ether. After the drying procedure, we got a purpose thing.

2.2. Preparation of liposome

The lipid mixture prepared using the constant ratio was dissolved in organic solvent. It was prepared by the conventional lipid-film method. The resulting liposomes were extruded

* Corresponding author. Tel.: +81 29 853 3220; fax: +81 29 853 3214.
E-mail address: m0720347@md.tsukuba.ac.jp (M. Shirakawa).

0969-8043/$ - see front matter © 2009 Elsevier Ltd. All rights reserved.
doi:10.1016/j.apradiso.2009.03.101

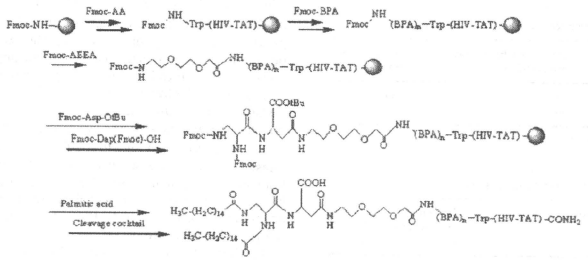

Fig. 1. Synthesis of the HIV-TAT and BPA peptide conjugated lipid analog.

Table 1
Composition of B5-TAT-lpopeptide modified liposome.

	DSPC	Cholesterol	DSPE-PEG2000	Bn-TAT-peptide
Plain liposome	50	50	–	–
PEG-liposome	47	47	6	–
B5-TAT5% PEG-liposome	45	45	5	5
B5-TAT10% PEG-liposome	42.5	42.5	5	10

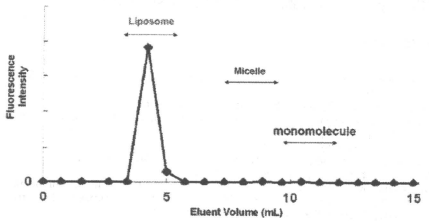

Fig. 2. Gel filtration chromatography of liposome, micelle, and monomolecule.

through polycarbonate membrane using an extruder, yielding the peptide-modified liposome (Table 1).

2.3. Gel filtration chromatography

The prepared liposome was subjected to size exclusion chromatography, which separated the liposome, micelle and monomolecule fractions, and the content of the lipopeptide was determined (Fig. 2). The liposome was then measured using the fluorescence of the tryptophan residue of the lipopeptide.

3. Results

3.1. Identification of lipopeptide

In the case of $n = 5$ (B5-TAT), the C8-column used for high performance liquid chromatography (HPLC) analysis showed the main peak (retention time at 13.6 min) accompanied by the existence of some impurities (Fig. 3a). However, the synthesis of conjugated lipopeptide attached to palmitoyl chain as an anchor

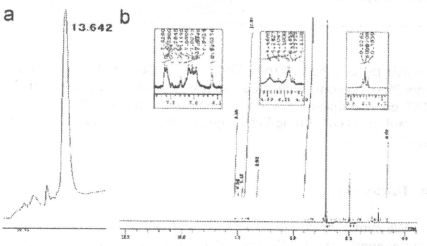

Fig. 3. Identification of HIV-TAT peptide and BPA conjugated lipid analog B5-TAT. (a) C8-HPLC, (b) ^{1}H NMR.

domain proceeded very smoothly. HPLC analysis showed almost one peak, and ESI-TOFMS (electrospray ionization mass spectroscopy) showed m/z 3504 of the dehydration peak as an exact mass of m/z 3522. In addition, ^{1}H NMR analysis (JEOL JMN-AL400) also showed the structure of the lipopeptide; for example, the molar ratio of the TAT-peptide and palmitoyl moiety showed the correct proton ratio of the ortho position on the tyrosine residue (2H as a characteristic signal of the peptide at 6.62 ppm) to the methyl signal at 0.81 ppm in the alkyl chain end (6H as a characteristic signal of the lipid) using an integration value of ^{1}H NMR spectra (Fig. 3b). The overall yield of the lipopeptide was greater than 70% based on the molar ratio of the amino group on TGS-RAM resin.

3.2. Incorporated ratio of lipopeptide

The incorporation of lipopeptide into the liposome was examined. Synthesized lipopeptide was incorporated into the liposome effectively. The incorporated ratios of lipopeptide to liposome are summarized in Table 2.

3.3. Physical properties of liposomes

We examined the diameter of the liposomes with monodispersion and zeta-potential by means of dynamic light scattering measurement (Zetasizer Nano ZS, Malvern Instruments Ltd.) liposomes, which were composed of DSPC, cholesterol, DSPE-PEG, and the lipopeptide were prepared by the lipid-film method followed by extrusion. The diameters of the liposomes were

Table 2
Liposome formation and lipopeptide incorporated into liposome.

Lipopeptide	Theoretical lipopeptide ratio (mol%)	Incorporated ratio (%)
B5-TAT lipopeptide	5	66.1
	10	73.4

Table 3
Physicochemical property of functionalized liposome.

DSPC/Chol/DSPE-PEG/B-TAT (molar ratio)		Particle size (nm, u/ G2)	Zeta potential (mV)
Plain liposome	50/50/0/0	147	−40
PEG-liposome	47/47/6/0	143	−15
B3-TAT lipopeptide liposome	45/45/5/5	120.3	17.5
	42.5/42.5/5/10	101.3	20.7
B5-TAT lipopeptide liposome	45/45/5/5	105.9	21
	42.5/42.5/5/10	147.8	26.4

shown to be about 100 nm. The positive charge of the peptide-modified liposome indicated the presence of basic peptide HIV-TAT on the liposome surface. The characteristics of liposomal formulations containing BPA conjugate peptide are summarized in Table 3.

4. Discussion

We synthesized a new peptide lipid containing multiple BPA components and a TAT domain for use in a boron-containing liposome which can encapsulate a boron compound in its internal water phase. The peptide lipid can be efficiently incorporated into liposomes that are 100 nm in diameter.

HIV-TAT was first developed from reverse transcriptase of HIV. It is a kind of protein transduction domain (Green and Loewenstein, 1998) which can introduce intracellular protein, deoxyribonucleic acid and macromolecular-containing liposome (Wadia et al., 2004; Eric and Steven, 2004; Fretz et al., 2005). Yagi et al. reported an in vitro anti-tumor effect of DOX encapsulated by TAT-modified liposome in 2007 (Yagi et al., 2007). The TAT-conjugating liposome facilitated an in vitro gene expression as well as in vivo expression when the same liposome was locally injected (Torchilin et al., 2003).

Active targeting against tumor cells using TAT have been evaluated; however, there is no previous report involving a boron-containing TAT liposome or compound.

A sufficient concentration of boron is necessary for successful BNCT. Thus, a material with high boron content generally has an advantage (Maruyama et al., 2004). Nakamura et al. developed a double-stranded boron cluster in 2004 (Lee et al., 2007). In the present study, the peptide lipid synthesized contains only 1–5 boron in a single molecule. However, our peptide lipid allows the number of boron to be increased up to $n = 12$ or 15.

In general, the hydrophilic charge of BSH in a boron-containing liposome has certain difficulty in encapsulating more BSH in the internal water phase of the liposome itself. There has been no previous report involving encapsulated BSH in the internal water phase within a boron liposome. Our peptide modification liposome of the hydrophilic charge is aspartic acid, and it shows high performance in terms of film stability and has a potential advantage in encapsulating BSH in the liposome in which the lipopeptide conjugate BPA.

Further investigation is needed to determine the in vitro and in vivo toxicity and the boron introduction efficiency.

5. Conclusions

We succeeded in synthesizing a lipopeptide containing boron. This lipopeptide could be incorporated into the liposome effectively. After toxicity testing, these liposomes will be administered to the cells or in vivo as a new BDS candidate.

Acknowledgments

This study was supported in part by a grant-in aid from the Ministry of Health, Labour and Welfare (WGA22039).

References

Barth, R.F., Coderre, J.A., Vicente, M.G., Blue, T.E., 2005. Clin. Cancer Res., 3987–4002.
Eric, L.S., Steven, F.D., 2004. Pharm. Res. 21 (3), 389–393.
Fretz, M.M., Mastrobattista, E., Koning, G.A., Jiskoot, W., Storm, G., 2005. Int. J. Pharm. 298 (2), 305–309.
Green, M., Loewenstein, P.M., 1998. Cell 55 (6), 1179–1888.
Lee, J.-D., Ueno, M., Miyajima, Y., Nakamura, H., 2007. Org. Lett. 9, 323–326.
Locher, G.L., 1936. Am. J. Roentgenol. 36, 1–13.
Maruyama, K., Ishida, O., Kasaoka, S., Takizawa, T., Utoguchi, N., Shinohara, A., Chiba, M., Kobayashi, H., Eriguchi, 2004. J. Controlled Release 98, 195–207.
Nakamura, H., 2008. Yakugaku zasshi 128 (2), 193–208.
Solid-phase Synthesis Handbook. Merk.
Soloway, A.H., Tjarks, W., Barnum, B.A., Rong, F-G., Barth, R.F., Codogni, I.M., Wilson, J.G., 1998. Chem. Rev. 98, 1515–1562.
Torchilin, V.P., Levchenko, T.S., Rammohan, R., Volodina, N., Papahadjopoulos-Sternberg, B., D'Souza, G.G.M., 2003. Proc. Natl. Acad. Sci. USA 100 (4), 1972–1977.
Vives, E., 2003. J. Mol. Recognit. 16, 265–271.
Wadia, J.S., Stan, R.V., Dowdy, S.F., 2004. Nat. Med. 10 (3), 310–315.
Yagi, N., Ogawa, Y., Kodaka, M., Okada, T., Tomohiro, T., Konakahara, T., Okuno, H., 2000. Lipids 20, 673–679.
Yagi, N., Yano, Y., Hatanaka, K., Yokoyama, Y., Okuno, H., 2007. Biomed. Lett. 17, 2590–2593.

Applied Radiation and Isotopes 67 (2009) S94–S96

Contents lists available at ScienceDirect

Applied Radiation and Isotopes

journal homepage: www.elsevier.com/locate/apradiso

Intracellular uptake of a new boronated porphyrin EC032

T. Tsurubuchi, T. Yamamoto *, K. Nakai, A. Zaboronok, F. Yoshida, M. Miyakawa, M. Shirakawa, Y. Yamamoto, M. Matsuda, A. Matsumura

Department of Neurosurgery, Institute of Clinical Medicine, University of Tsukuba, Japan

ARTICLE INFO

Keywords:
Boronated porphyrin
Fluorescence study
ICP-AES
^{10}B concentration

ABSTRACT

We measured the toxicity and intracellular uptake of a newly developed boronated porphyrin EC032, and verified the fluorescence-based boron concentration measuring methods. Toxicity study showed that concentration required to produce a 50% reduction in viability (IC_{50}) of EC032 was more than 0.25 mM. Fluorescence study showed the intracellular uptake of EC032 increased up until 24 h after its exposure to C6, 9L, U87, and U251 cells. There was also a linear correlation between ICP-AES and fluorescence intensity as an arbitrary unit about measurement of boron concentration.

Fluorescence-based boron concentration measuring methods are very simple and useful methods, especially for screening of slight test dose of porphyrin compounds.

1. Introduction

To improve the therapeutic effect of BNCT, sufficient amount of boron and neutron delivery in tumor tissue is important. Several tumor selective porphyrin compounds such as ATN-10 (Yamamoto et al., 1998), STA-BX909 (Matsumura et al., 1999) have been reported in our group. We measured the toxicity and intracellular uptake of a newly developed boronated porphyrin EC032 as a new boron carrier. This compound has a tumor selective porphyrin unit and also has a cage of boron (Fig. 1). The fluorescence-based ^{10}B concentration measuring methods was verified.

2. Materials and methods

2.1. Toxicity study

Cytotoxicity effects of EC032 on tumor cells such as C6, 9L rat gliosarcoma cells, and U87, U251 human glioblastoma cells were examined using [3-(4,5-dimethylthiazol-2-yl)-5-(3carboxymethoxyphenyl)-2-(4-sulphophenyl)-2H-tetrazolium, inner salt] (MTS) assay in comparison with sodium borocaptate (BSH) under dark condition. The tumor cells were dispensed into 96-well microplate at a concentration of 5×10^3 cells/100 μl of supplemented Dulbecco's modified Eagle's medium. The plates were incubated at 37 °C in a humidified CO_2 incubator for 48 h before the addition of EC032 or BSH. The concentration of EC032 or BSH ranged from 0.25 μM to 2.5 mM. The same series of dilutions was prepared without addition of cells as background control samples. The plates were incubated for an additional 48 h after which the medium was changed and 20 μl of cell titer 96 aqueous assay system from Promega was added to each sample's well. The absorbance was measured in a microplate reader at 490 nm after 1.5 h. The concentration required to produce a 50% reduction in viability (IC_{50}) was determined.

2.2. Fluorescence study

C6, 9L, U87, U251 cells were incubated with 20 μM EC032 in conditioned medium for 30 min, 1 h, 2 h, 6 h, and 12 h in a 96-well microplate. The cultured medium was washed three times with PBS. The cells were pipetted and minced with Triton-X. The fluorescence intensity as an arbitrary unit (a.u.) of the sample in the well was measured by microplate reader. The excitation wave length was 405 nm and the emission wave length was 670 ± 10 nm. Cells of the same condition were trypsinized and counted. Then the intracellular uptake of EC032 was determined. All experimental procedures were done under dark condition.

2.3. Measurement of boron concentration

We evaluated the correlation between inductively coupled plasma atomic emission spectroscopy (ICP-AES) and fluorescence intensity (a.u.) detected by microplate reader. C6, 9L, U87, and U251 cells were incubated with BSH or with EC032, which were, respectively, added to the conditioned medium at a boron concentration of 30 μg/ml. The incubation times were 6 and 24 h. The cultures were washed once with PBS. The cells were counted

* Corresponding author. Tel.: +81 298 533220; fax: +81 298 533214.
E-mail address: tetsu-ya@md.tsukuba.ac.jp (T. Yamamoto).

0969-8043/$ - see front matter © 2009 Elsevier Ltd. All rights reserved.
doi:10.1016/j.apradiso.2009.03.098

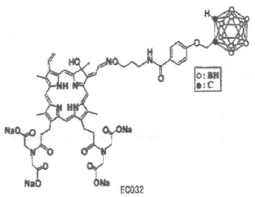

Fig. 1. Constitutional formula of EC032.

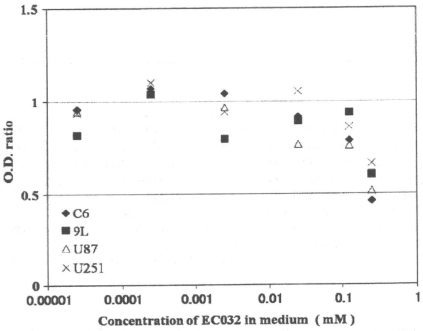

Fig. 2. Toxicity study of EC032 using MTS assay.

and pretreated by wet ashing method. Then the intracellular boron concentration was measured by ICP-AES. Using another part of the same sample for the measurement of the concentration of EC032, the fluorescence intensity (a.u.) of the sample was measured by microplate reader under dark condition.

3. Results

Toxicity study: The IC_{50} of EC032 was more than 0.25 mM in 9L, U87, U251, C6 cells (Fig. 2).

The IC_{50} of BSH was more than 0.25 mM in U87 and U251 cells and less than 0.25 mM in 9L, C6 cells (Fig. 3).

Fluorescence study: The intracellular uptake of EC032 increased until 24 h after its exposure to C6, 9L, U87, and U251 cells (Fig. 4).

Boron concentrations in cultured glioma cells (C6, 9L, U87, and U251) in the wells of a 96-well microplate after 24 h incubation with EC032 are shown in Table 1.

Measurement of boron concentration: There was a linear correlation between ICP-AES and fluorescence intensity (a.u.) regarding the measurement of boron concentration (Fig. 5).

4. Discussion

As a new boron carrier, EC032 shows low toxicity and time-dependent increase until 24 h in many glioma cell lines. Fluorescence-based measurement of boron concentration is a very simple and useful method.

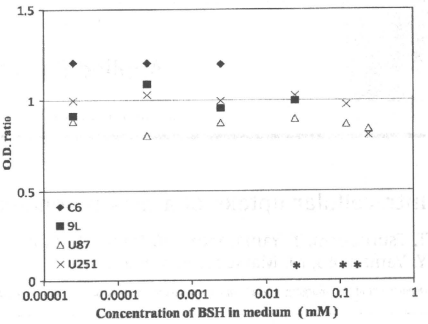

Fig. 3. Toxicity study of BSH using MTS assay. An asterisk means the IC50 of BSH beyond 0.0125 mM is not detectable. Double asterisks means the IC50 of BSH beyond 0.125 mM is not detectable.

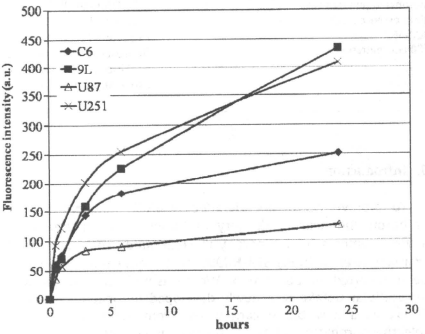

Fig. 4. Fluorescence study of EC032 in vitro.

Table 1
Boron concentration in cultured glioma cells (C6, 9L, U87, U251) in the well of 98-well microplate after 24 h incubation with EC032.

C6	9L	U87	U251
0.4141 (μg B) per 3996 cells	0.2245 (μg B) per 4500 cells	0.4087 (μg B) per 2760 cells	0.2700 (μg B) per 2316 cells

BSH and boronophenylalanine (BPA) are well known boron carriers which have been widely used in recent boron neutron capture therapy. The toxicity of BSH (Mares et al., 1992) and BPA (Barth et al., 2004) are known to be very low. No drug has been reported with lower toxicity than these drugs. However, a few studies about the cytotoxicity of BSH *in vitro* have been reported. The IC_{50} of EC032 was more than 0.25 mM, which has lower toxicity than the other boron porphyrins and boron compounds (Barth et al., 2004). This indicates that EC032 has low toxicity under dark condition. The IC_{50} of BSH was more than 0.25 mM other than C6 and 9L cells in this study. These data were slightly

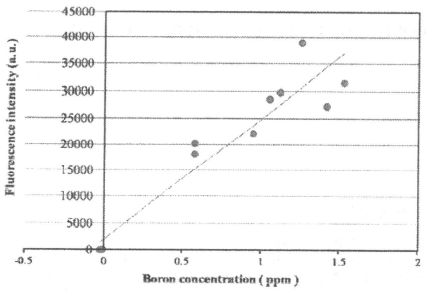

Fig. 5. Linear correlation between boron concentration (ppm) measured by ICP-AES and fluorescence intensity (a.u.) ($R = 0.95404$).

lower than previous data (Mares et al., 1992). One reason is perhaps that the IC_{50} values of BSH in C6, 9L cells were underestimated because of the clearance of live cells, which decreased their adhesion ability due to ultrastructual changes under high concentrations of BSH (Mares et al., 2003). Another is the differences in cellular characteristics among the cell lines.

Serial changes of the intracellular concentration of EC032 in many tumor cell lines showed a time-dependent increase up until 24 h. According to the report by (Yoshida et al., 2002), BSH shows a homogeneous but low boron concentration pattern in tumor tissues, and BPA shows a heterogeneous but high boron concentration pattern. The uptake pattern of other boronated porphyrins such as porpyrin-cobaltacarborane (Hao et al., 2007), meso-tetra(4-nido-carboranylphenyl)porphyrin (Vincente et al., 2002) in tumor cells resembles that with our compound EC032. Other boronated compound such as boronated porphyrin (BOPP) showed an uptake and retention at least 20 times that of BSH (Fairchild et al., 1990; Ceberg et al., 1995). Although the tumor cell lines and cell numbers are different among these experiments, the estimated intracellular uptake of EC032 seems to be more than that of BOPP (Hill et al., 1992; Nguyen et al., 1993). Many porphyrin compounds have characteristics suitable for drug targeting because of their affinity to LDL receptors (Spizzirri et al., 1996; Shibata et al., 2001; Novick et al., 2006), localization in the intracellular lysosome (Callahan et al., 1999), and quantitative detection with fluorescence techniques. Further study of *in vivo* tissue uptake is warranted to determine the appropriate administration dose of EC032 to get acceptable tumor selectivity.

There is a linear correlation between the fluorescence intensity (a.u.) measured by microplate reader and the boron concentration measured by ICP-AES. Measurement of the boron concentration using ICP-AES is a widely used reliable method; our result indicates the reliability of fluorescence-based measurement of boron concentration in tumor cells. Moreover, our method is simpler and more convenient than other methods like prompt gamma ray methods and ICP-AES, especially for screening of low test doses of boron compounds.

The new porphyrin EC032 showed low toxicity and time-dependent increase and quantitative results with a fluorescence microplate reader. Therefore, EC032 is a candidate for a boron carrier in boron neutron capture therapy.

5. Conclusion

The new boronated porphyrin EC032 has low cytotoxicity and shows time-dependent uptake in tumor cells. Fluorescence-based boron concentration measuring methods are very simple and useful methods, especially for screening of low test dose of porphyrin compounds.

Acknowledgments

This study was supported in part by a Grant-in-Aid from the Ministry of Education, Science and Culture, Japan (20390379).

References

Barth, R.F., Yang, W., Al-Madhoun, A.S., Johnsamuel, J., Byun, Y., Chandra, S., Smith, D.R., Tjarks, W., Eriksson, S., 2004. Boron-containing nucleosides as potential delivery agents for neutron capture therapy of brain tumors. Cancer Res. 64 (1), 6287–6295.

Callahan, D.E., Forte, T.M., Afzal, S.M.J., Deen, D.F., Kahl, S.B., Bjornstad, K.A., Bauer, W.F., Blakely, E.A., 1999. Boronated protoporphyrin (BOPP): localization in lysosomes of the human glioma cell line SF-767 with uptake modulated by lipoprotein levels. Int. J. Radiat. Oncol. Biol. Phys. 45 (3), 761–771.

Ceberg, C.P., Brun, A., Kahl, S.B., Koo, M.S., Person, B.R., Salford, L.G.A., 1995. A cooparative study on the pharmacokinetics and biodistribution of boronated porphyrin (BOPP) and sulfhydryl boron hydride (BSH) in the RG2 rat glioma model. J. Neurosurg. 83, 86–92.

Fairchild, R.G., Kahl, S.B., Laster, B.H., J. Kalef-Ezra, J., Popenoe, E.A., 1990. In vitro determination of uptake, retention, distribution, biological efficacy, toxicity of boronated compounds for neutron capture therapy: a comparison of porphyrins with sulfhydryl boron hydrides. Cancer Res. 50, 4860–4865.

Hao, E., Sibrian-Vazquez, M., Serem, W., Garno, J.C., Fronczek, F.R., Vincente, M.G.H., 2007. Synthesis, aggregation and cellular investigation of porphyrin-cobalta-carborane conjugates. Chem. Eur. J. 13, 9035–9042.

Hill, J.S., Kahl, S.B., Kaye, A.H., Stylli, S.S., Koo, M., Gonzales, M.F., Vardaxis, N.J., Johhson, C.I., 1992. Selective tumor uptake of boronated porphyrin in an animal model of cerebral glioma. PNAS 89, 1785–1789.

Mares, V., Baudysova, M., Kvitek, J., Hnatowicz, V., Cervena, J., Vacik, J., Folbergrova, J., 1992. Accumulation of boron-10 in cell cultures exposed to ercaptodode-caborate used for the neutron capture therapy. J. Pharmacol. Exp. Therapeutics. 262, 818–822.

Mares, V., Krajci, D., Lisa, V., 2003. Subcellular targets of mercaptoborate (BSH), a carrier of 10B for neutron capture therapy (BNCT) of brain tumors. Physiol. Res. 52 (5), 629–635.

Matsumura, A., Shibata, Y., Yamamoto, T., Yoshida, F., Isobe, T., Nakai, K., Hayakawa, Y., Kiri, M., Shimojo, N., Ono, K., Sakata, I., Nakajima, S., Okumura, M., Nose, T., 1999. A new boronated porphyrin (STA-BX909) for neutron capture therapy: an in vitro survival assay and in vivo tissue uptake study. Cancer Lett. 141, 203–209.

Nguyen, T., Brownell, G.L., Holden, S.A., Teicher, B.A., 1993. Intracellular distribution of various boron compounds for use in boron neutron capture therapy. Biochem. Pharmacol. 45 (1), 147–155.

Novick, S., Laster, B.H., Quastel, M.R., 2006. Postitive cooperativity in the cellular uptake of a boronated porphyrin. Int. J. Biochem. Cell Biol. 38, 1374–1381.

Shibata, Y., Matsumura, A., Yoshida, F., Yamamoto, T., Nakai, K., Nose, T., Sakata, I., Nakajima, S., 2001. Competitive uptake of porphyrin and LDL via the LDL receptor in glioma cell lines: flow cytometric analysis. Cancer Lett. 166 (1), 79–87, 10.

Spizzirri, P.G., Hill, J.S., Kahl, S.B., Ghiggino, K.P., 1996. Photophysics and intracellular distribution of a boronated porphyrin phototherapeutic agent. Photochem. Photobiol. 64 (6), 975–983.

Vincente, M.G.H., Edwards, B.F., Shetty, S.J., Hou, Y., Boggan, J.E., 2002. Syntheses and preliminary biological studies of four meso-tetra(nido-carboranylmethyl)-phenylporphyrins. Bioorg. Med. Chem. 10, 481–492.

Yamamoto, T., Matsumura, A., Shibata, Y., Fujimori, H., Nakai, K., Yoshida, F., Nose, T., Sakata, T., Nakajima, S., Miwa, N., 1998. Manganese-metalloporphyrin (ATN-10) as a tumor-localizing agent: magnetic resonance imaging and inductively coupled plasma atomic emission spectroscopy study with experimental brain tumors. Neurosurgery 42 (6), 1332–1338.

Yoshida, F., Matsumura, A., Shibata, Y., Yamamoto, T., Nakauchi, H., Okumura, M., Nose, T., 2002. Cell cycle dependence of boron uptake from two boron compounds used for clinical neutron capture therapy. Cancer Lett. 187 (1–2), 135–141, 10.

Glycobiology vol. 19 no. 7 pp. 735–742, 2009
doi:10.1093/glycob/cwp041
Advance Access publication on March 17, 2009

Involvement of chondroitin sulfate E in the liver tumor focal formation of murine osteosarcoma cells

Basappa[2,3,8], Sengottuvelan Murugan[2,3], Kazuki N Sugahara[4,5], Chun Man Lee[4,6], Gerdy B ten Dam[7], Toin H van Kuppevelt[7], Masayuki Miyasaka[4], Shuhei Yamada[1,3], and Kazuyuki Sugahara[1,3]

[3]Graduate School of Life Science, Hokkaido University, Sapporo, Japan; [4]Laboratory of Immunodynamics, Department of Microbiology and Immunology, Osaka University, Graduate School of Medicine, Suita, Japan; [5]Vascular Mapping Center, Burnham Institute for Medical Research UCSB, University of California, Santa Barbara, CA, USA; [6]Medical Center for Translational Research, Osaka University Hospital, Suita, Japan; [7]Department of Biochemistry, Nijmegen Centre for Molecular Life Sciences, Radboud University Nijmegen Medical Centre, Nijmegen, The Netherlands; and [8]Department of Chemistry, Bangalore University, Bangalore, India

Received on December 26, 2008; revised on March 10, 2009; accepted on March 12, 2009

Cell surface heparan sulfate plays a critical role in regulating the metastatic behavior of tumor cells, whereas the role of chondroitin sulfate/dermatan sulfate (CS/DS) has been little understood in this context. Here, we characterized CS/DS chains from the murine osteosarcoma cell line LM8G7, which forms tumor nodules in liver. Structural analysis of the CS/DS chains showed a higher proportion of GlcUAβ1-3GalNAc(4,6-*O*-disulfate) (E-units) in LM8G7 (12%) than in its parental cell line LM8 (6%), which rarely forms tumors in the liver. Immunostaining with GD3G7, an antibody specific to E-units, confirmed the higher expression of the epitope in LM8G7 than LM8 cells. The tumor focal formation of LM8G7 cells in the liver in mice was effectively inhibited by the preadministration of CS-E (rich in E-unit) or the preincubation of the antibody GD3G7 with the tumor cells. CS-E or GD3G7 inhibited the adhesion of LM8G7 cells to a laminin-coated plate in vitro. In addition, the invasive ability of LM8G7 cells in vitro was also reduced by the addition of CS-E or the antibody. Further, CS-E or the antibody inhibited the proliferation of LM8G7 cells dose dependently. The binding of LM8G7 cells to VEGF in vitro was also significantly reduced by CS-E and GD3G7. Thus, the present study reveals the significance of highly sulfated CS/DS structures in the liver colonization of osteosarcoma cells and also provides a framework for the development of GAG-based anticancer molecules.

Keywords: chondroitin sulfate/glycosaminoglycan/osteosarcoma/sulfation/tumor

Introduction

The metastatic cascade consists of various interactions between tumor cells and the host cells or components of the extracellular matrix (ECM) and involves migration, adhesion, and invasion, which are mediated by cell surface molecules (Fidler 2003). Proteoglycans (PGs), a class of cell surface adhesion molecules composed of glycosaminoglycan (GAG) side chains attached to core proteins, are expressed in the ECM, and have diverse functions including roles in growth factor-binding, cell–ECM interactions, cell–cell adhesion, cell proliferation, differentiation, and tissue morphogenesis and embryogenesis (Liotta 1986; Esko and Selleck 2002). Heparan sulfate (HS) or chondroitin sulfate (CS)/dermatan sulfate (DS) side chains modulate the interaction of tumor cells with host cells and ECM components (Gallagher 1989; Iida et al. 1996) and play a critical role in regulating tumor initiation, progression, and metastasis (Sanderson 2001; Munesue et al. 2007).

The GAGs in normal tissues differ in quantity and type from those found during embryonic development and in tumors (Dietrich 1984). It has become increasingly clear that heterogeneity in the structure of HS is important in regulating disease processes including cancer (Nakanishi et al. 1992). Elevated levels of CS have also been reported in transformed cells (Lv et al. 2007). Alterations in the CS structure in tumors have been correlated with an increase in malignancy (Iida et al. 1998). In animal experiments, chondroitinase (CSase) treatment slowed the progression of cancer, leading to the suggestion that CS-PGs on the surface of cancer cells are useful therapeutic targets (Denholm et al. 2001).

In addition to ECM components, malignant cells produce a variety of soluble factors such as tumor necrosis factor-α, vascular endothelial growth factor (VEGF), and heparin-binding epidermal growth factor-like growth factor (HB-EGF), which play a major role in tumor progression (Jayne et al. 2000). Among these, VEGF and its receptors, VEGFR-1 and VEGFR-2, are more highly expressed in a metastatic model than in nonmetastatic neoplasms and directly correlate with the extent of neovascularization and degree of proliferation (Takahashi et al. 1995). Generally, it is assumed that these growth factors and other signaling proteins drive the oncogenic process through direct/indirect interactions with cell surface molecules.

Cell surface molecules such as HS regulate the signal transduction of tumor cells by interacting with various growth factors such as fibroblast growth factor-2 (FGF-2) (Mundhenke et al. 2002), VEGF (Iozzo and San Antonio 2001), and HB-EGF (Chu et al. 2005). Likewise, a rare highly sulfated GlcUAβ1-3GalNAc(4S, 6S) structure (the E-unit) in CS/DS chains, where 4S and 6S stand for 4-*O*- and 6-*O*-sulfate, respectively, plays an important role in the interaction of various functional proteins (growth factors/cytokines) (Deepa et al. 2002). In addition, the

[1]To whom correspondence should be addressed: Tel: +81-(11)-706-9055; Fax: +81-(11)-706-9055; e-mail: tjohej@sci.hokudai.ac.jp and k-sugar@sci.hokudai.ac.jp

[2]These authors contributed equally to this work.

Table I. Disaccharide composition of CS/DS chains in osteosarcoma cell lines LM8 and LM8G7[a]

Unsaturated disaccharide	LM8, pmol (mol%)	LM8G7, pmol (mol%)
ΔO: ΔHexUA-GalNAc	65.7 (64.9)	50.4 (55.8)
ΔC: ΔHexUA-GalNAc(6S)	13.0 (12.8)	7.4 (8.6)
ΔA: ΔHexUA-GalNAc(4S)	15.8 (15.8)	21.4 (23.7)
ΔD: ΔHexUA(2S)-GalNAc(6S)	N.D.[d]	N.D.
ΔB: ΔHexUA(2S)-GalNAc(4S)	N.D.	N.D.
ΔE: ΔHexUA-GalNAc(4S, 6S)	6.6 (6.5)	10.7 (11.9)
ΔT: ΔHexUA(2S)-GalNAc(4S, 6S)	N.D.	N.D.
Total[b]	101.2 (100)	90.0 (100)
S/unit[c]	0.41	0.55
Molar ratio of the total disaccharides[e]	1.12:1.00	

[a]The GAG preparation from each osteosarcoma cell line was digested with CSase ABC, and the digest was analyzed by anion-exchange HPLC after labeling with a fluorophore 2-AB as described in *Material and methods*.
[b]Amounts of disaccharides/mg of dried cells.
[c]A molar ratio of sulfate to disaccharide.
[d]N.D., not detected.
[e]A molar ratio of the total CS/DS disaccharides of the two cell lines.

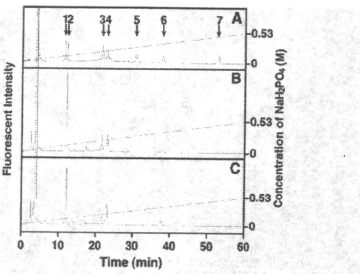

Fig. 1. Anion-exchange HPLC of CSase ABC digests of the CS/DS chains obtained from the osteosarcoma cell lines LM8 and LM8G7. The CS/DS preparations were digested individually with CSase ABC. After 2AB-labeling, each digest was analyzed by HPLC on an amine-bound silica PA-03 column using a linear gradient of NaH_2PO_4 as indicated by the dashed line. The peaks before 10 min were derived from 2AB-derivatizing reagents. (**A**) Authentic hyaluronan/CS-derived unsaturated disaccharides. (**B**) and (**C**) 2AB-labeled CS-derived unsaturated disaccharides obtained from LM8 and LM8G7 cells, respectively. Arrows indicate the elution positions of the 2AB-derivatized authentic hyaluronan and CS disaccharides: (1) $\Delta^{4,5}$HexUA-GlcNAc; (2) $\Delta^{4,5}$HexUA-GalNAc; (3) $\Delta^{4,5}$HexUA-GalNAc(6S); (4) $\Delta^{4,5}$HexUA-GalNAc(4S); (5) $\Delta^{4,5}$HexUA(2S)-GalNAc(6S); (6) $\Delta^{4,5}$HexUA-GalNAc(4S, 6S); (7) ΔHexUA(2S)-GalNAc(4S, 6S).

involvement of E-units in various biological functions such as neurite outgrowth (Sugahara and Mikami 2007), bone formation, and biomineralization has been reported (Miyazaki et al. 2008). However, the involvement of highly sulfated structures of CS/DS chains in the process of tumor formation in different organ sites is not well understood.

Recently, we reported the involvement of CS structures containing E-units in the metastasis of a Lewis lung carcinoma cell line (Li et al. 2008). An analysis of liver-specific tumor phenotypes has revealed the overexpression or specific structural changes of HS chains to be critical to the metastatic potential of melanoma cells (Tóvári et al. 1997). These findings prompted us to examine whether structural differences in the CS/DS chains of osteosarcoma cells explain the metastatic potential. In the present study, we demonstrated that the E-unit-containing structure of CS/DS chains in murine osteosarcoma LM8G7 cells is involved in the liver tumor focal formation.

Results

Comparison of CS/DS chains between LM8 and LM8G7 cells

The amount and composition of the unsaturated disaccharides produced by digestion with CSase ABC from the CS/DS polysaccharide chains, which had been extracted from LM8 and LM8G7 cells, are tabulated in Table I, and the representative anion-exchange HPLC chromatograms for the disaccharide analyses are shown in Figure 1. The amounts of CS/DS in LM8G7 and LM8 cells were comparable. Upon digestion with CSase ABC, CS/DS chains from both the cell lines yielded $\Delta^{4,5}$HexUAα1-3GalNAc (ΔO-unit), $\Delta^{4,5}$HexUAα1-3GalNAc(6S) (ΔC-unit), $\Delta^{4,5}$HexUAα1-3GalNAc(4S) (ΔA-unit), and $\Delta^{4,5}$HexUAα1-3GalNAc(4S, 6S) (ΔE-unit) in varying proportions. The degree of sulfation of CS/DS chains was relatively higher (0.55) in LM8G7 cells than in LM8 cells (0.41) (Table I). The proportion of the highly sulfated disaccharide ΔE-unit was higher in LM8G7 cells (12%) than LM8 cells (6%). The proportion of ΔC-units was significantly lower in LM8G7 cells (9%) than in LM8 cells (13%), whereas the proportion of ΔA-units was higher in LM8G7 cells (24%) than LM8 cells (16%).

In view of the recent finding of a higher proportion of E-units in the highly metastatic Lewis lung carcinoma cell line LM66-H11 than in the low metastatic cell line P29 (Li et al. 2008), it was speculated that the higher proportion of E-units in the CS/DS preparation of LM8G7 cells may be a key factor in the tumor focal formation in the liver. To confirm the overexpression of E-units on the surface of LM8G7 cells, a phage display antibody (GD3G7) specific to CS-E (Purushothaman et al. 2007; ten Dam et al. 2007; Li et al. 2008) was used for the immunostaining of the osteosarcoma cell lines. LM8G7 cells were more strongly stained by GD3G7 than were LM8 cells (Figure 2), suggesting higher levels of the expression of the E-unit.

Characterization of antitumor activity of CS isoforms

To examine the involvement of CS/DS in the liver tumor focal formation, various commercial CS preparations such as CS-A, CS-C, and CS-E (100 μg) were individually preinjected into mice 30 min before the intravenous injection of LM8G7 cells. Among the CS preparations tested, CS-E characterized by a high proportion (62%) of E-units (Kinoshita et al. 1997) completely inhibited the colonization of LM8G7 cells (Figure 3D), suggesting the importance of the E-unit in the tumor focal formation in the liver. Dose-dependent inhibition experiments showed that CS-E inhibited the tumor focal formation of LM8G7 cells strongly at 100 or 150 μg but not at all at low doses (25 or 50 μg) (Figure 4A). Heparin, a well-known antitumor agent (Borsig et al. 2001), also inhibited the liver colonization of LM8G7 cells (Figure 3G), whereas CS-A or CS-C failed to inhibit it (Figure 3B and C).

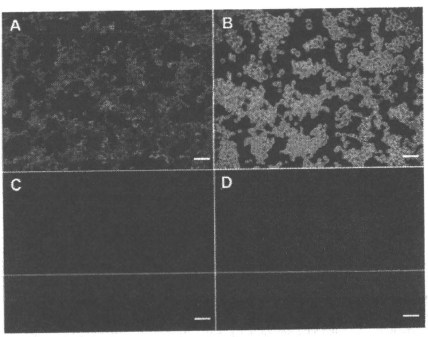

Fig. 2. Immunocytological detection of the GD3G7 epitope on the surface of murine osteosarcoma LM8 and LM8G7 cells. LM8 (**A**) and LM8G7 (**B**) cells were seeded separately on chamber slides, cultured for 24 h, and fixed with Diff-Quick reagent A. They were incubated with the antibody GD3G7 for 1 h, and bound GD3G7 was detected with an anti-VSV glycoprotein antibody followed by an Alexa-conjugated third antibody and visualized by confocal microscopy. In control experiments, LM8G7 cells were stained without GD3G7 (**C**) or irrelevant antibody MPB49V (**D**). Scale bar, 100 μm.

Antitumor activity of the antibody GD3G7

The higher expression of E-units on the surface of LM8G7 cells and the strong antitumor activity of CS-E led us to hypothesize that E-unit-containing CS/DS chains on the tumor cell surface are involved in the liver tumor focal formation. It should be noted that the colonization of LM8G7 cells is specific to the liver, and no tumor colony formation was observed in other mouse organs including the lungs (data not shown). To test our hypothesis, the antibody GD3G7, which recognizes E-unit-containing CS/DS chains, was used for antitumor assays. The preincubation of LM8G7 cells with the antibody (0.2–2 μg) for 30 min strongly inhibited the liver tumor focal formation in a dose-dependent manner (Figures 3E and 4B), whereas the irrelevant antibody MPB49V (2 μg) failed to inhibit it (Figure 3F and 3G), suggesting that the epitopes for the antibody GD3G7 play a key role in the liver colonization of LM8G7 cells.

Effects of CS-E and GD3G7 on adhesion and invasion of LM8G7 cells

Effects of CS-A, CS-E (50 μg), or the antibody GD3G7 (2 μg) on the adhesion of LM8G7 cells to a laminin-coated plate were examined. Laminin, a major basement membrane protein, plays an important role in the interaction of tumor cells with the basement membrane during the extravasation step of metastasis (Baba et al. 2008). CS-E and the antibody GD3G7 inhibited the adhesion of LM8G7 cells to the substrate (Figure 5). In contrast, CS-A or the control antibody MPB49V had no effect on the attachment of LM8G7 cells to laminin.

Since the adhesion of tumor cells to basement membranes is an initial step in the invasion process, it was examined whether the antitumor effects of CS-E and GD3G7 are also due to the inhibition of cell invasion. The effects of CS-A, CS-C, CS-E (50 μg), or GD3G7 (2 μg) on the invasion by LM8G7 cells of Matrigel™ were tested. The invasive ability of the cells was reduced by CS-E and the antibody, but CS-A and CS-C had no significant effect (Figure 6). These results indicate CS-E-like epitopes to be involved in the invasion by LM8G7 cells as well.

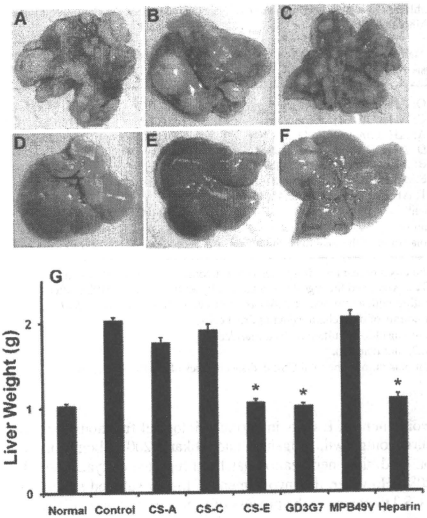

Fig. 3. Effects of CS isoforms and the antibody GD3G7 on the liver tumor focal formation of LM8G7 cells. The CS/DS preparation (100 μg) in 200 μL of Dulbecco's Modified Eagle's Medium (DMEM) was injected into a tail vein of C3H/HeN mouse 30 min before the injection of LM8G7 cells (1×10^6). LM8G7 cells were also preincubated with the antibody GD3G7 (2 μg) or the control antibody MPB49V (2 μg) for 30 min at 37°C and used for the tumor colonization experiments. Representative livers from the mice treated with DMEM (Control) (**A**), CS-A (**B**), CS-C (**C**), CS-E (**D**), antibody GD3G7 (**E**), or MPB49V (**F**) are shown. The average liver weight of the control and treated mice (**G**). Heparin from porcine intestinal mucosa (100 μg) was used as a positive control. The data represent mean values ± SD for two independent experiments. $^*P < 0.01$ versus control. Mann–Whitney U test.

Effects of CS-E and the antibody GD3G7 on the proliferation of LM8G7 cells

To examine the effects of GAGs and GD3G7 on cell proliferation, LM8G7 cells (5×10^3) were seeded and CS-A (100 μg), CS-C (100 μg), CS-E (50–150 μg), heparin (100 μg), or an antibody (2–5 μg) in DMEM containing 10% FBS was added. CS-E and GD3G7 inhibited the proliferation in a dose-dependent manner (Figure 7), whereas CS-A and CS-C showed no effect. Heparin, as a positive control, inhibited the proliferation of LM8G7 cells. These observations led us to conclude that CS/DS chains at the cell surface play a major role in the proliferation of tumor cells.

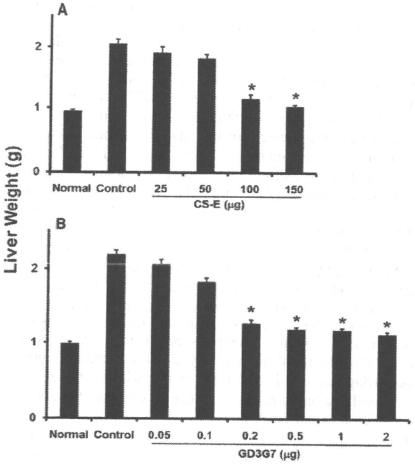

Fig. 4. Dose-dependent antitumor activity of CS-E and the antibody GD3G7. (**A**) The antitumor activity of various doses (25, 50, 100, or 150 μg) of CS-E was investigated as described in the legend to Figure 2. (**B**) LM8G7 cells were preincubated with the antibody GD3G7 at different doses (0.05, 0.1, 0.2, 0.5, 1, or 2 μg) for 30 min and used for the analysis of tumor focal formation as described in the legend to Figure 2. Six mice were used per group. The data represent mean values ± SD for two independent experiments. $^{*}P < 0.01$ versus control. Mann-Whitney *U* test.

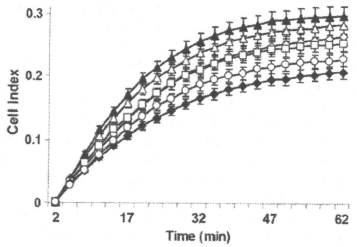

Fig. 5. Real-time monitoring of the effects of CS-A, CS-E, or GD3G7 on the adhesion of LM8G7 cells to the laminin substrate. LM8G7 cells (2×10^4) were seeded in ACEA's 96× e-plate™ coated with (△) or without laminin (◇), and the effects of CS-A (50 μg, ▲), CS-E (50 μg, ○), GD3G7 (2 μg, ◇), and MPB49V (2 μg, □) were observed for 60 min using the RT-CES™ system as described in *Material and methods*. The cell index (quantitative measurement of cells in a well containing an electrode) values were plotted against time. The data represent mean values ± SD for three independent experiments.

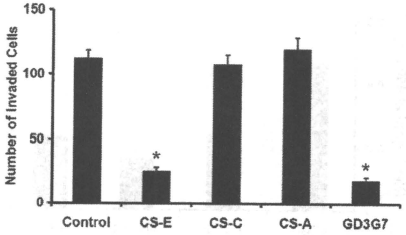

Fig. 6. Effects of various CS isoforms and the antibody GD3G7 on the invasion of LM8G7 cells. (A) The invasion of LM8G7 cells (2.5×10^4) was measured using a BD BioCoat™ chamber (BD Biosciences) coated with Matrigel™ in the presence or absence of CS-A, CS-C, CS-E (50 μg), or GD3G7 (2 μg) in the upper chamber and allowed to invade through the Matrigel for 24 h. The cell invasion was measured as described in *Material and methods*. The number of invaded cells is presented. The data represent mean values ± SD for two independent experiments. $^{*}P < 0.01$ versus control. Mann–Whitney *U* test.

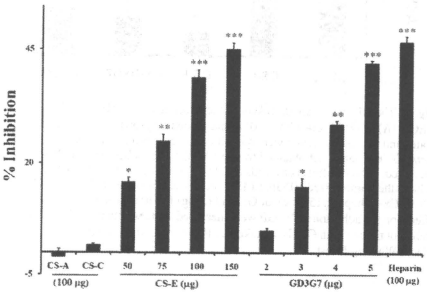

Fig. 7. Effects of various GAGs and the antibody GD3G7 on the proliferation of LM8G7 cells. (A) LM8G7 cells (5×10^3) were plated on 96-well plates in DMEM supplemented with 10% fetal bovine serum (FBS) in the presence or absence of CS-A (100 μg), CS-C (100 μg), CS-E (50 to 150 μg), heparin (100 μg), or the antibody GD3G7 (2 or 5 μg). The number of viable cells was determined 3 days after seeding. The data represent mean values ± SD for three independent experiments. $^{*}P < 0.01$ versus control. $^{**}P < 0.05$ versus control. Mann–Whitney *U* test.

Comparison of the binding of LM8G7 cells to various growth factors

VEGF, expressed by tumor cells, facilitates the progression of cancer (Asai et al. 1998). We examined the ability of LM8G7 cells to bind growth factors in vitro. LM8G7 cells interacted well with VEGF, FGF-2, midkine (MK), and hepatocyte growth factor (HGF), but the degree of binding was the greatest with VEGF (Figure 8A). The attachment of LM8G7 cells to VEGF was strongly inhibited by the addition of CS-E or the antibody GD3G7 but not inhibited by CS-A or CS-C. Heparin, a positive control, also inhibited the attachment of LM8G7 cells to VEGF (Figure 8B).

Discussion

PGs associated with the surface of cancer cells have been recognized as important in a variety of cancers (Blackhall et al. 2001). Alterations in the level of expression of the GAG structure and/or

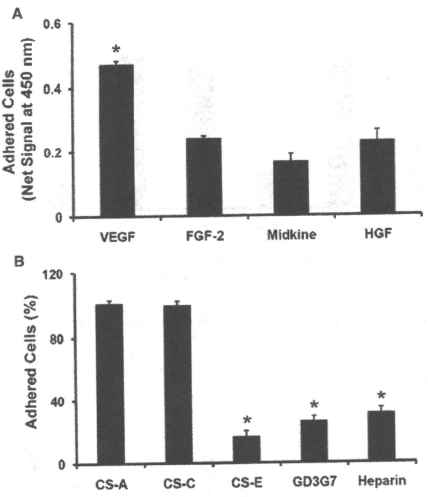

Fig. 8. The effects of various GAGs on the attachment of LM8G7 cells to VEGF. (**A**) LM8G7 cells (2.5×10^4) were seeded on growth factor-coated plates and the cells attached were quantified as described in *Material and methods*. The net signal obtained for the LM8G7 cells adhered to VEGF is presented. (**B**) The effects of GAGs or GD3G7 on the attachment of LM8G7 cells to the immobilized VEGF. LM8G7 cells were preincubated with CS-A, CS-C, CS-E, heparin (50 μg), or GD3G7 (2 μg) for 30 min at 37°C, and their effects on the adhesion of VEGF were measured. Values obtained with control wells not treated with GAGs are taken as 100%. $^*P < 0.01$ versus control. Mann–Whitney *U* test.

density on PGs can potentially make cancer cells highly versatile in modulating their behavior. For instance, significant changes in the PG content and GAG structure in tumors have been reported (Theocharis 2002). It has been demonstrated that the disaccharide composition of cell surface HS varies during the transition from human colon adenoma to carcinoma (Jayson et al. 1998). Low-sulfated HS facilitates metastasis through the adhesion of hepatoma cells to the ECM (Robinson et al. 1984). In addition, low levels of cell surface HS are correlated well with the high metastatic activity of many tumors (Redini et al. 1986; Kure et al. 1987; Sugahara et al. 1989; Timar et al. 1992).

This study revealed heterogeneous yet unique structures in the CS/DS chains of LM8 and LM8G7 cells. The major disaccharide present in LM8 and LM8G7 cells was the unsulfated unit, levels of which were lower in LM8G7 than LM8 cells. An important finding of this study was the higher proportion of E-units in the CS/DS chains of LM8G7 than LM8 cells. In addition, LM8G7 cells were more strongly immunostained by the antibody GD3G7 than were LM8 cells, supporting the increased expression of E-units in LM8G7 cells. The results of our study indicate the correlation between highly sulfated CS structures and the metastatic potential of osteosarcoma cells. To investigate the relationship between the CS-E-like-structures and the liver tumor focal formation, various CS isoforms including CS-E were administered into mice to evaluate their effects against the colonization of LM8G7 cells. Animals preinjected with CS-E had no tumor nodules in the liver, but the mice injected with other CS isoforms had tumor nodules, indicating the antitumor role of CS-E. In addition, the antibody GD3G7 completely inhibited the tumor forming activity of LM8G7 cells in the liver, suggesting the involvement of the GD3G7 epitope containing E-units in the liver tumor focal formation of LM8G7 cells. These results are consistent with our recent finding that the experimental metastasis of the mouse Lewis lung carcinoma cell line involves the E-unit-containing epitope on the cell surface and is strongly inhibited by exogenous CS-E and the antibody GD3G7. It has also been reported that the epitope structure of GD3G7 is highly expressed in human ovarian carcinomas (ten Dam et al. 2007) and human pancreatic tumors (Sugahara et al. 2008). However, it remains to be established whether E-unit-containing structures are involved in the natural metastasis of human tumors. A high-throughput survey using tissue microarrays for the epitope of the antibody GD3G7 in natural human tumors (Sugahara et al. 2008) will clarify whether the epitope can be used as a tumor marker for diagnosis and is a therapeutic target of certain cancers.

Tumor formation in the distinct organs has been suggested to be essential for the development of metastasis. To investigate the mechanistic basis for the antitumor activity of CS-E against LM8G7 cells, we performed adhesion, invasion, and proliferation experiments in vitro to validate the effects of CS isoforms on the liver tumor focal formation of LM8G7 cells. We dynamically monitored the attachment of tumor cells to the laminin-coated plate in the presence or absence of CS isoforms or the antibody GD3G7. Both CS-E and GD3G7 markedly inhibited the attachment of LM8G7 cells to the laminin-coated plate. Therefore, it is reasonable to hypothesize that the preadministration of CS-E may weaken tumor cell adhesion to endothelial cells thereby preventing the liver colonization. Further, the invasive ability of LM8G7 cells was significantly reduced by CS-E, but not by the other isoforms. Supporting this observation, GD3G7 also strongly inhibited the invasion by LM8G7 cells. Next, we tested the effects of CS-A, CS-C, CS-E, or GD3G7 on cell proliferation. CS-E and GD3G7 inhibited the proliferation of LM8G7 cells in a dose-dependent manner. These results suggest the E-unit-containing epitopes to be involved in the tumor forming process and a potential target for the diagnosis and treatment of osteosarcoma tumors.

It is well known that VEGF-releasing metastatic tumor cells dysregulate the endothelial cell–cell junctional complex upon binding and facilitates tumor extravasation (Weis et al. 2004). In this study, the addition of CS-E or GD3G7 strongly inhibited the interaction of tumor cells with VEGF. The most plausible explanation for this inhibition would be the direct binding of soluble CS-E to immobilized VEGF thereby preventing the attachment of tumor cells to VEGF, since it has been reported that highly sulfated CS-E interacts with VEGF in vitro (ten Dam et al. 2007). These results may also explain the inhibitory effects of CS-E on the liver colonization of LM8G7 cells. Thus, the present study reveals the significance of highly sulfated CS/DS structures in the liver tumor focal formation of the osteosarcoma cells and also provides a framework for the development of GAG-based anticancer molecules (Yamada and Sugahara 2008).

Material and methods

Materials

Standard unsaturated CS disaccharides, CSase ABC (EC 4.2.2.4), CS-A from whale cartilage, CS-C from shark cartilage, and CS-E from squid cartilage, and cell proliferation assay kit, TetraColor One, were purchased from Seikagaku Corp. (Tokyo, Japan). Recombinant human (rh)-HGF was from PeproTech EC Ltd (London, UK). rh-VEGF-165, rh-FGF-2, and rh-MK were obtained from Wako Pure Chemicals Co. (Osaka, Japan). The single chain antibody GD3G7 was selected for reactivity with rat embryo-derived GAGs by the phage display technique (ten Dam et al. 2007). The monoclonal anti-vesicular stomatitis virus glycoprotein (VSV-G) tag antibody P5D4 was from Sigma (St. Louis, MO). Porcine intestinal mucosal heparin was obtained from Nacalai Tesque (Kyoto, Japan). Alexa Fluor 488-conjugated goat anti-mouse IgG (H+L) was obtained from Invitrogen. Actinase E was from Kaken Pharmaceutical Co. (Tokyo, Japan). Mouse sarcoma laminin from the basement membrane of Engelbreth-Holm Swarm was obtained from Sigma. 2-Aminobenzamide (2AB) was purchased from Nacalai Tesque (Kyoto, Japan). Sodium cyanoborohydride ($NaBH_3CN$) was from Aldrich Chemical Co. (Milwaukee, WI). 100× nonessential amino acids, β-mercaptoethanol, 100× sodium pyruvate, the cell dissociation buffer, and L-glutamine were from GIBCO (Auckland, New Zealand). The Diff-Quick solution was from International Reagent Corp. (Kobe, Japan). All other chemicals and reagents were of the highest quality available.

Animals and cell lines

Nine-week-old female C3H/HeN mice were obtained from Japan SLC (Hamamatsu, Japan) and kept in standard housing. All the experiments were performed according to protocols approved by the local animal care committee of Hokkaido University. The murine osteosarcoma cell line LM8G7, which has high metastatic potential to liver, was cloned from LM8G5 cells (Lee et al. 2002) as described (Fidler and Nicolson 1976) and cultured in DMEM supplemented with 10% (v/v) FBS (Thermo Trace, Melbourne, Australia), streptomycin (100 μg/mL), penicillin (100 units/mL), 100× nonessential amino acids, β-mercaptoethanol (50 μM), 100× sodium pyruvate, and L-glutamine (2 mM) at 37°C in a humidified 5% CO_2 atmosphere. The cells were harvested after being incubated with 0.1% trypsin/1 mM EDTA in phosphate-buffered saline (PBS) for 5 min at 37°C, gently flushed with a pipette, and subcultured three times a week.

Extraction of GAGs from LM8 and LM8G7 cells

Cells were dehydrated and delipidated by extraction with acetone, air-dried, and used for the extraction of GAGs essentially as previously described (Li et al. 2007) with some modifications. Briefly, the acetone powder was digested with heat-activated (60°C, 30 min) actinase E in 200 μL of 0.1 M sodium borate, pH 8.0, containing 10 mM calcium acetate at 60°C for 48 h. After the incubation, each sample was treated with 5% trichloroacetic acid and kept for 30 min at 4°C. The precipitate was removed by centrifugation. The supernatant was extracted with diethyl ether to remove the trichloroacetic acid. After neutralization with 1.0 M sodium carbonate, the aqueous phase was adjusted to contain 80% ethanol and 1% sodium acetate, and kept at 4°C overnight. The precipitated crude GAGs were recovered by centrifugation, desalted on a PD-10 column (GE Healthcare, Buckinghamshire, UK) using the 50 mM pyridine acetate buffer, pH 5.0, as an eluent, and evaporated dry.

Analysis of the disaccharide composition of CS chains

The disaccharide composition of GAG preparations from the osteosarcoma cell lines was determined as described (Li et al. 2007). Briefly, the samples were dissolved in water, and an aliquot was digested with CSase ABC (Saito et al. 1968) and labeled with 2AB (Kinoshita and Sugahara 1999). The excess 2AB was removed by extraction with chloroform (Kawashima et al. 2002). The 2AB-labeled digest was analyzed by anion-exchange HPLC on a PA-03 silica column (YMC-Pack PA, Kyoto, Japan) with a linear gradient of NaH_2PO_4 from 16 to 538 mM over 60 min at a flow rate of 1.0 mL/min at room temperature. Identification and quantification of the resulting disaccharides were achieved by comparison with the elution of authentic CS-derived unsaturated disaccharides (Kinoshita and Sugahara 1999).

Immunocytochemistry

To detect the E-unit-containing epitopes, murine osteosarcoma cell lines, LM8 and LM8G7, were stained using a phage display single chain antibody, GD3G7 (Purushothaman et al. 2007; ten Dam et al. 2007). Briefly, osteosarcoma cells were plated on 8-well Lab-Tech chamber slides (Nalge Nunc International, Roskilde, Denmark), cultured for 24 h, and fixed with Diff-Quick reagent A. After being blocked with PBS containing 3% bovine serum albumin (BSA) for 1 h at room temperature, the fixed cells were incubated with 100 μL of the primary antibody GD3G7 (diluted 1:100 (10 μg/mL) in 0.1% BSA/PBS) for 1 h at room temperature and washed with PBS. After being incubated with the anti-VSV-G antibody (diluted 1:5,000 in 0.1% BSA/PBS) for 1 h at room temperature, the cells were washed with PBS. To detect the anti-VSV-G antibody, the cells were stained with a third antibody conjugated to Alexa Fluor 488 (diluted 1:5000 in 0.1% BSA/PBS) and visualized with a laser-scanning confocal microscope, FLUOVIEW (Olympus, Tokyo, Japan).

Assay of liver tumor focal formation

In preparation for injection, LM8G7 cells were harvested after a brief exposure to a cell dissociation buffer (GIBCO) and the cell viability in single-cell suspensions was determined by trypan blue exclusion. A total of 1×10^6 cells suspended in 200 μL of DMEM were injected into a lateral tail vein of C3H/HeN mice. Four weeks later, the animals were sacrificed. The number of visible tumor cell nodules in the liver was examined and liver weight was recorded.

To elucidate the involvement of cell surface CS/DS in the liver tumor focal formation, the C3H/HeN mice received 100 μg of commercial CS preparations (CS-A, CS-C, or CS-E) or heparin 30 min before the tumor cell injection. The dose-dependent inhibition experiments were carried out using CS-E (25, 50, 100, or 150 μg). In other instances, to investigate the involvement of the antibody GD3G7 epitope in the liver tumor focal formation, LM8G7 cells were preincubated with serially diluted GD3G7 (0.05, 0.1, 0.2, 0.5, 1, or 2 μg) or the irrelevant antibody MPB49V (2 μg) for 30 min at 37°C. Aliquots of the cell

suspension were assessed for cell viability before the injection. After incubated with antibodies (GD3G7 or MPB49V) and prior to the injection of the tumor cells into animals, it was ensured by microscopic observations that these cells were in a single cell suspension.

Real-time monitoring of the adhesion of LM8G7 cells to the laminin substrate

The cell attachment assay was carried out using the RT-CES™ system (ACEA Biosciences, San Diego, CA). ACEA's 96× microtiter plates were coated with laminin (0.5 μg/well) at 37°C for 1 h. Attachment and spreading of LM8G7 cells (2×10^4) were monitored in the presence or absence of various inhibitors such as CS-A (50 μg), CS-E (50 μg), the antibody GD3G7 (2 μg), or the control antibody MPB49V (2 μg), and continuously monitored for up to 62 min using the RT-CES™ system. The cell index (quantitative measurement of cells in a well containing an electrode) was plotted against time.

Cell invasion assay in vitro

The invasion of LM8G7 cells across the Matrigel™-coated porous membranes was assessed using a 24-well plate (8 μm pore size, insert size: 6.4 μm) (BD Biosciences, Franklin Lakes, NJ) according to the manufacturer's protocol. Briefly, single cell suspensions of LM8G7 cells (2.5×10^4) were prepared by detaching and resuspending the cells in DMEM containing 0.1% BSA. Before the cells were added, the chambers were rehydrated for 2 h in an incubator at 37°C. The lower chambers were filled with DMEM containing 5% FBS. In some instances, LM8G7 cells (2.5×10^4) in serum-free DMEM were preincubated with CS-A, CS-C, CS-E (50 μg), or the antibody GD3G7 (2 μg) for 30 min at 37°C in a CO_2 incubator and added to the upper chamber. After incubation for 24 h, cells that had passed through the Matrigel-coated membrane and remained attached to the opposite surface of the membrane were stained with the Diff-Quick solution and counted in five random microscopic fields per filter.

Assay of cell proliferation in vitro

To examine the effects of CS isoforms on proliferation in vitro, LM8G7 cells were seeded at a density of 5×10^3 cells/well in a 96-well plate and treated with CS-E (50–150 μg), GD3G7 (2–5 μg), CS-A (100 μg), CS-C (100 μg), or heparin (100 μg) for 3 days. After a specific period of time, 5 μL of TetraColor One (Tanaka et al. 2002) reagent was added and incubated for an additional 4 h, and the absorbance at 450 nm (Bio-Rad, Hercules, CA) was measured. The viability of the cells was expressed in percentage terms.

Tumor cell-growth factor adhesion assay

The adhesion of tumor cells to various growth factors (Hibino et al. 2005) in vitro was assessed in a 96-well plate. VEGF, FGF-2, MK, and HGF (100 ng) were added to the microtiter plate and incubated overnight at 4°C. After blocking the wells with 1% BSA in PBS, DMEM-containing LM8G7 cells (2.5×10^4) in 0.1% BSA were added to a plate and incubated for 1 h at 37°C in a humidified 5% CO_2 atmosphere. After a brief wash with PBS, 100 μL of PBS containing 5 μL of TetraColor One was added and the plate was incubated for 45 min. The viable adhered cells were quantified by measuring the absorbance at 450 nm. The net signal is obtained by subtracting the background obtained with a BSA-coated well. In other instances, the cells were preincubated with CS-A, CS-C, CS-E, heparin (50 μg), or GD3G7 (2 μg) for 30 min at 37°C and used for the experiment.

Acknowledgement

Basappa and Sengottuvelan Murugan are grateful to the Japan Society for the Promotion of Science (JSPS) for a postdoctoral fellowship.

Funding

The Ministry of Education, Culture, Sports, Science, and Technology of Japan (MEXT) (20390019), the New Energy and Industrial Technology Development Organization (NEDO) (to K.S.), the Human Frontier Science Program (RGP62/2004 to T.H.v.K.), the Dutch Cancer Society, grant number 2008-4058 (to G.t.D.).

Conflict of interest statement

None declared.

Abbreviations

$\Delta^{4,5}$HexUA, 4,5-unsaturated hexuronic acid; 2AB, 2-aminobenzamide; 4S, 4-*O*-sulfate; 6S, 6-*O*-sulfate; BSA, bovine serum albumin; CS, chondroitin sulfate; DMEM, Dulbecco's modified Eagle's medium; DS, dermatan sulfate; ECM, extracellular matrix; E-unit, GlcUAβ1-3GalNAc(4S, 6S); FBS, fetal bovine serum; FGF-2, fibroblast growth factor-2; GAG, glycosaminoglycan; GalNAc, *N*-acetyl-D-galactosamine; GlcUA, D-glucuronic acid; HB-EGF, heparin-binding epidermal growth factor-like growth factor; HexUA, hexuronic acid; HGF, hepatocyte growth factor; HS, heparan sulfate; MK, midkine; PBS, phosphate-buffered saline; VEGF, vascular endothelial growth factor.

References

Asai T, Ueda T, Itoh K, Yoshioka K, Aoki Y, Mori S, Yoshikawa H. 1998. Establishment and characterization of a murine osteosarcoma cell line (LM8) with high metastatic potential to the lung. *Int J Cancer.* 76:418–422.

Baba Y, Iyama KI, Hirashima K, Nagai Y, Yoshida N, Hayashi N, Miyanari N, Baba H. 2008. Laminin-332 promotes the invasion of oesophageal squamous cell carcinoma via PI3K activation. *Br J Cancer.* 98:974–980.

Blackhall FH, Merry CL, Davies EJ, Jayson GC. 2001. Heparan sulfate proteoglycans and cancer. *Br J Cancer.* 19:1094–1098.

Borsig L, Wong R, Feramisco J, Nadeau DR, Varki NM, Varki A. 2001. Heparin and cancer revisited: Mechanistic connections involving platelets, P-selectin, carcinoma mucins, and tumor metastasis. *Proc Natl Acad Sci USA.* 98:3352–3357.

Chu CL, Goerges AL, Nugent MA. 2005. Identification of common and specific growth factor binding sites in heparan sulfate proteoglycans. *Biochemistry.* 44:12203–12213.

Deepa SS, Umehara Y, Higashiyama S, Itoh N, Sugahara K. 2002. Specific molecular interactions of oversulfated chondroitin sulfate E with various heparin-binding growth factors. Implications as a physiological binding partner in the brain and other tissues. *J Biol Chem.* 277:43707–43716.

Denholm EM, Lin YQ, Silver PJ. 2001. Anti-tumor activities of chondroitinase AC and chondroitinase B: Inhibition of angiogenesis, proliferation and invasion. *Eur J Pharmacol.* 416:213–221.

Dietrich CP. 1984. A model for cell–cell recognition and control of cell growth mediated by sulfated glycosaminoglycans. *Braz J Med Biol Res.* 17:5–15.

Esko JD, Selleck SB. 2002. Order out of chaos: Assembly of ligand binding sites in heparan sulfate. *Annu Rev Biochem.* 71:435–471.

Fidler IJ. 2003. The pathogenesis of cancer metastasis: The "seed and soil" hypothesis revisited. *Nat Rev Cancer.* 3:453–458.

Fidler IJ, Nicolson GL. 1976. Organ selectivity for implantation survival and growth of B16 melanoma variant tumor lines. *J Natl Cancer Inst.* 57:1199–11202.

Gallagher JT. 1989. The extended family of proteoglycans: Social residents of the pericellular zone. *Curr Opin Cell Biol.* 1:1201–1218.

Hibino S, Shibuya M, Hoffman MP, Engbring JA, Hossain R, Mochizuki M, Kudoh S, Nomizu M, Kleinman HK. 2005. Laminin alpha5 chain metastasis- and angiogenesis-inhibiting peptide blocks fibroblast growth factor 2 activity by binding to the heparan sulfate chains of CD44. *Cancer Res.* 65:10494–10501.

Iida J, Meijne AM, Knutson JR, Furcht LT, McCarthy JB. 1996. Cell surface chondroitin sulfate proteoglycans in tumor cell adhesion, motility and invasion. *Semin Cancer Biol.* 7:155–162.

Iida J, Meijne AM, Oegema TR Jr, Yednock TA, Kovach NL, Furcht LT, McCarthy JB. 1998. A role of chondroitin sulfate glycosaminoglycan binding site in alpha4beta1 integrin-mediated melanoma cell adhesion. *J Biol Chem.* 273:5955–5962.

Iozzo RV. 1998. Matrix proteoglycans: From molecular design to cellular function. *Annu Rev Biochem.* 67:609–652.

Iozzo RV, San Antonio JD. 2001. Heparan sulfate proteoglycans: Heavy hitters in the angiogenesis arena. *J Clin Invest.* 108:349–355.

Jayne DG, Perry SL, Morrison E, Farmery SM, Guillou PJ. 2000. Activated mesothelial cells produce heparin-binding growth factors: Implications for tumour metastases. *Br J Cancer.* 82:1233–1238.

Jayson GC, Lyon M, Paraskeva C, Turnbull JE, Deakin JA, Gallagher JT. 1998. Heparan sulfate undergoes specific structural changes during the progression from human colon adenoma to carcinoma in vitro. *J Biol Chem.* 273:51–57.

Kawashima H, Atarashi K, Hirose M, Hirose J, Yamada S, Sugahara K, Miyasaka M. 2002. Oversulfated chondroitin/dermatan sulfates containing GlcAbeta1/IdoAalpha1-3GalNAc(4,6-*O*-disulfate) interact with L- and P-selectin and chemokines. *J Biol Chem.* 277:12921–12930.

Kinoshita A, Sugahara K. 1999. Microanalysis of glycosaminoglycan-derived oligosaccharides labeled with a fluorophore 2-aminobenzamide by high-performance liquid chromatography: Application to disaccharide composition analysis and exosequencing of oligosaccharides. *Anal Biochem.* 269:367–378.

Kinoshita A, Yamada S, Haslam SM, Morris HR, Dell A, Sugahara K. 1997. Novel tetrasaccharides isolated from squid cartilage chondroitin sulfate E contain unusual sulfated disaccharide units GlcA(3-*O*-sulfate)beta1-3GalNAc(6-*O*-sulfate) or GlcA(3-*O*-sulfate)beta1-3GalNAc. *J Biol Chem.* 272:19656–19665.

Kure S, Yoshie O, Aso H. 1987. Metastatic potential of murine B16 melanoma correlates with reduced surface heparan sulfate glycosaminoglycan. *Jpn J Cancer Res.* 78:1238–1245.

Lee CM, Tanaka T, Murai T, Kondo M, Kimura J, Su W, Kitagawa T, Ito T, Matsuda H, Miyasaka M. 2002. Novel chondroitin sulfate-binding cationic liposomes loaded with cisplatin efficiently suppress the local growth and liver metastasis of tumor cells in vivo. *Cancer Res.* 62:4282–4288.

Li F, Shetty AK, Sugahara K. 2007. Neuritogenic activity of chondroitin/dermatan sulfate hybrid chains of embryonic pig brain and their mimicry from shark liver. Involvement of the pleiotrophin and hepatocyte growth factor signaling pathways. *J Biol Chem.* 282:2956–2966.

Li F, ten Dam GB, Murugan S, Yamada S, Hashiguchi T, Mizumoto S, Oguri K, Okayama M, van Kuppevelt TH, Sugahara K. 2008. Involvement of highly sulfated chondroitin sulfate in the metastasis of the Lewis lung carcinoma cells. *J Biol Chem.* 283:34294–34304.

Liotta LA. 1986. Tumor invasion and metastases – Role of the extracellular matrix. *Cancer Res.* 46:1–7.

Lv H, Yu G, Sun L, Zhang Z, Zhao X, Chai W. 2007. Elevate level of glycosaminoglycans and altered sulfation pattern of chondroitin sulfate are associated with differentiation status and histological type of human primary hepatic carcinoma. *Oncology.* 72:347–356.

Miyazaki T, Miyauchi S, Tawada A, Anada T, Matsuzaka S, Suzuki O. 2008. Oversulfated chondroitin sulfate-E binds to BMP-4 and enhances osteoblast differentiation. *J Cell Physiol.* 217:769–777.

Mundhenke C, Meyer K, Drew S, Friedl A. 2002. Heparan sulfate proteoglycans as regulators of fibroblast growth factor-2 receptor binding in breast carcinomas. *Am J Pathol.* 160:185–194.

Munesue S, Yoshitomi Y, Kusano Y, Koyama Y, Nishiyama A, Nakanishi H, Miyazaki K, Ishimaru T, Miyaura S, Okayama M, et al. 2007. A novel function of syndecan-2, suppression of matrix metalloproteinase-2 activation, which causes suppression of metastasis. *J Biol Chem.* 282:28164–28174.

Nakanishi H, Oguri K, Yoshida K, Itano N, Takenaga K, Kazama T, Yoshida A, Okayama M. 1992. Structural differences between heparan sulphates of proteoglycan involved in the formation of basement membranes in vivo by Lewis-lung-carcinoma-derived cloned cells with different metastatic potentials. *Biochem J.* 288:215–224.

Purushothaman A, Fukuda J, Mizumoto S, ten Dam GB, van Kuppevelt TH, Kitagawa H, Mikami T, Sugahara K. 2007. Functions of chondroitin sulfate/dermatan sulfate chains in brain development. Critical roles of E and iE disaccharide units recognized by a single chain antibody GD3G7. *J Biol Chem.* 282:19442–19452.

Redini F, Moczar E, Poupon MF. 1986. Cell surface glycosaminoglycans of rat rhabdomyosarcoma lines with different metastatic potentials and of non-malignant rat myoblasts. *Biochim Biophys Acta.* 883:98–105.

Robinson J, Viti M, Höök M. 1984. Structure and properties of an under-sulfated heparan sulfate proteoglycan synthesized by a rat hepatoma cell line. *J Cell Biol.* 98:946–953.

Saito H, Yamagata T, Suzuki S. 1968. Enzymatic methods for the determination of small quantities of isomeric chondroitin sulfates. *J Biol Chem.* 243:1536–1542.

Sanderson RD. 2001. Heparan sulfate proteoglycans in invasion and metastasis. *Semin Cell Dev Biol.* 12:89–98.

Sugahara K, Mikami T. 2007. Chondroitin/dermatan sulfate in the central nervous system. *Curr Opin Struct Biol.* 17:536–545.

Sugahara K, Okumura Y, Yamashina I. 1989. The Engelbreth-Holm-Swarm mouse tumor produces undersulfated heparan sulfate and oversulfated galactosaminoglycans. *Biochem Biophys Res Commun.* 162:189–197.

Sugahara KN, Hirata T, Tanaka T, Ogino S, Takeda M, Terasawa H, Shimada I, Tamura J, ten Dam GB, van Kuppevelt TH, et al. 2008. Chondroitin sulfate E fragments enhance CD44 cleavage and CD44-dependent motility in tumor cells. *Cancer Res.* 68:7191–7199.

Takahashi Y, Kitadai Y, Bucana CD, Cleary KR, Ellis LM. 1995. Expression of vascular endothelial growth factor and its receptor, KDR, correlates with vascularity, metastasis, and proliferation of human colon cancer. *Cancer Res.* 55:3964–3968.

Tanaka Y, Nakayamada S, Fujimoto H, Okada Y, Umehara H, Kataoka T, Minami Y. 2002. H-Ras/mitogen-activated protein kinase pathway inhibits integrin-mediated adhesion and induces apoptosis in osteoblasts. *J Biol Chem.* 277:21446–21452.

ten Dam GB, van de Westerlo EM, Purushothaman A, Stan RV, Bulten J, Sweep FC, Massuger LF, Sugahara K, van Kuppevelt TH. 2007. Antibody GD3G7 selected against embryonic glycosaminoglycans defines chondroitin sulfate-E domains highly up-regulated in ovarian cancer and involved in vascular endothelial growth factor binding. *Am J Pathol.* 171:1324–1333.

Theocharis AD. 2002. Human colon adenocarcinoma is associated with specific post-translational modifications of versican and decorin. *Biochim Biophys Acta.* 1588:165–172.

Timar J, Ladanyi A, Lapis K, Moczar M. 1992. Differential expression of proteoglycans on the surface of human melanoma cells characterized by altered experimental metastatic potential. *Am J Pathol.* 141:467–474.

Tóvári J, Paku S, Rásó E, Pogány G, Kovalszky I, Ladányi A, Lapis K, Tímár J. 1997. Role of sinusoidal heparan sulfate proteoglycan in liver metastasis formation. *Int J Cancer.* 71:825–831.

Weis S, Cui J, Barnes L, Cheresh D. 2004. Endothelial barrier disruption by VEGF-mediated Src activity potentiates tumor cell extravasation and metastasis. *J Cell Biol.* 167:223–229.

Yamada S, Sugahara K. 2008. Potential therapeutic application of chondroitin sulfate/dermatan sulfate. *Curr Drug Discov Technol.* 5:289–301.

Int. J. Cancer: **125,** 2316–2322 (2009)

Enhanced expression of Annexin A4 in clear cell carcinoma of the ovary and its association with chemoresistance to carboplatin

Ayako Kim[1,2], Takayuki Enomoto[1], Satoshi Serada[2], Yutaka Ueda[1], Tsuyoshi Takahashi[2,3], Barry Ripley[2], Takashi Miyatake[1], Masami Fujita[1], Chun Man Lee[4], Koji Morimoto[5], Minoru Fujimoto[2], Tadashi Kimura[1] and Tetsuji Naka[2]*

[1]*Department of Obstetrics and Gynaecology, Osaka University Graduate School of Medicine, Osaka, Japan*
[2]*Laboratory for Immune Signal, National Institute of Biomedical Innovation, Osaka, Japan*
[3]*Department of Surgery, Osaka University Graduate School of Medicine, Osaka, Japan*
[4]*Medical Center for Translational Research, Osaka University Hospital, Osaka, Japan*
[5]*Department of Breast and Endocrine Surgery, Osaka University Graduate School of Medicine, Osaka, Japan*

Clear cell carcinoma (CCC) of the ovary is known to be highly resistant to platinum-based chemotherapy. The purpose of our study was to identify a candidate protein that is associated with chemoresistance of CCC and to investigate the specific mechanism of chemoresistance conferred by the identified protein. Enhanced expression of Annexin A4 (Anx A4) was identified in ovarian CCC cells using 2-D differential gel electrophoresis (2D-DIGE) and mass spectrometry. Anx A4 levels were elevated in CCC cells compared with non-CCC cells as determined by real-time RT-PCR and Western blot analysis. Immunohistochemical analysis of Anx A4 was performed in 126 epithelial ovarian cancer tissue samples and demonstrated significantly elevated levels of Anx A4 protein levels in ovarian CCC tumors compared with ovarian serous and endometrioid tumors ($p < 0.01$). Anx A4-transfected ovarian non-CCC cells were more resistant to carboplatin (IC50 = 42 μM) compared with control cells (IC50 = 23 μM) as determined by modified MTT assay. Intracellular platinum levels were significantly lower in Anx A4-transfected cells compared with control cells after carboplatin treatment ($p = 0.0020$) and after an additional 360 min of carboplatin-free incubation ($p = 0.0004$), as measured by atomic absorption spectrophotometry. Expression of Anx A4 is elevated in ovarian CCC tumors and is associated with chemoresistance in cultured ovarian cancer cells. These results demonstrate that Anx A4 confers chemoresistance in ovarian cancer cells in part by enhancing drug efflux. Thus, Anx A4 may represent a novel therapeutic target of chemoresistance in patients with ovarian CCC.

Key words: clear cell carcinoma of the ovary; chemoresistance; Annexin A4

Ovarian cancer is the 5th leading cause of cancer deaths for women in the United States, with approximately 21,600 new cases and 15,500 deaths reported annually.[1] In Japan, it is the eighth most common cause of cancer deaths, with approximately 7,700 new cases (2001) and 4,500 deaths (2007) reported yearly, and the incidence is increasing (Health, Labour and Welfare Ministry, Japan: Population Survey Report). More than 20% of all cases with ovarian cancer in Japan are classified as clear cell carcinoma (CCC) of the ovary, and for unknown reasons, this percentage is markedly higher (by approximately 2-fold) than in Europe and the United States.[2]

Because ovarian cancers (including ovarian CCC) are relatively asymptomatic at early stage, the majority of patients (approximately 70%) present with an advanced stage disease at first diagnosis and subsequently require surgical tumor reduction and adjuvant chemotherapy.[3,4] However, of the 4 major histological types of epithelial ovarian cancer, CCC of the ovary is highly resistant to conventional cancer chemotherapy (including carboplatin and paclitaxel treatment) compared with the other histological types.[2,5,6] Consequently, patients with ovarian CCC are associated with both poorer prognosis and higher mortality than patients with other types of ovarian cancer.[2] Thus, there is an urgent need to further our understanding of the pathogenesis of ovarian CCC, particularly with respect to the expression of proteins, which confer chemoresistance, for the development of a novel therapeutic strategy.

In this study, we performed a proteomic analysis using ovarian cancer cell lines [CCC for comparison with non-CCC serous adenocarcinoma (SAC)] to identify a candidate protein associated with chemoresistance in ovarian CCC. SAC was chosen as a control non-CCC cell line because of its chemosensitivity compared with the chemoresistant CCC cell line. We identified several proteins that are differentially upregulated in ovarian CCC compared with SAC and focused our investigation on Annexin A4 (Anx A4).

Anx A4 is an epithelial isoform of a ubiquitous family of soluble cytoplasmic proteins, which bind to and polymerize on the surface of cell membranes in response to increases in intracellular calcium.[7–9] Although the functions of Anx A4 have not been completely characterized, previous studies have identified major involvement of this protein in membrane permeability,[10] exocytosis[11,12] and regulation of ion channels.[13] Its roles in membrane fluidity and membrane trafficking may in part explain the involvement of Anx A4 in modulating drug resistance in cancer cells.

A previous report associating Anx A4 with chemoresistance in human cancer cell lines focused on human lung and colon cancer cell lines[14] but did not examine ovarian cancer cell lines. In addition, the mechanism of chemoresistance induced by Anx A4 has not been explored in detail. In the study of Morita *et al.*,[15] proteomic analysis showed enhanced expression of Anx A4 in the OVISE and OVTOKO ovarian CCC cell lines compared with the MCAS ovarian mucinous cancer cell line. However, a possible association between Anx A4 expression and chemoresistance was not investigated. Importantly, neither study tried to determine whether Anx A4 protein levels are elevated in tumors of patients with ovarian CCC.

In this study, we have addressed 2 important questions concerning Anx A4 and chemoresistance, *i.e.*, whether expression of Anx A4 is elevated in patient ovarian CCC tumors and by what mechanism Anx A4 confers chemoresistance.

Material and methods

Patients

We examined surgically obtained tumor tissue samples of 126 ovarian cancer patients (Table I) who underwent surgery at Osaka University Hospital, Japan, between 1999 and 2006. None of the patients entered in this study had received adjuvant chemotherapy, including paclitaxel or carboplatin treatment. Histologic features of the tissues were reviewed by board-certified pathologists. Diagnosis was based on the FIGO (International Federation of Gynecologists &

Grant sponsor: Japanese Ministry of Education, Science, Culture and Sports (Grants-Aids for Scientific Research).
***Correspondence to:** Laboratory for Immune Signal, National Institute of Biomedical Innovation, 7-6-8 Saito-asagi, Ibaraki, Osaka 567-0085, Japan. Fax: +81-72-641-9837. E-mail: tnaka@nibio.go.jp
Received 13 February 2009; Accepted after revision 12 May 2009
DOI 10.1002/ijc.24587
Published online 20 May 2009 in Wiley InterScience (www.interscience.wiley.com).

TABLE I – SUMMARY OF CLINICAL CHARACTERISTICS OF OVARIAN CANCER PATIENTS EXAMINED IN THIS STUDY

Histology	Mean age (range)	FIGO stages				Total
		I	II	III	IV	
CCC	53 (36–66)	27	5	9	2	43
Endometrioid	53 (28–66)	2	7	4	0	13
Mucinous	53 (28–90)	6	1	1	0	8
SAC	55 (33–81)	9	13	35	5	62
						126

Obstetricians) classification system. Patient profiles (age, FIGO stage) were analyzed against each of the 4 major epithelial ovarian cancer histological types (CCC, endometrioid adenocarcinoma, mucinous adenocarcinoma and serous adenocarcinoma). Written informed consent was obtained for all the cases, and the experimental protocol was approved by the ethics committee of Osaka University.

Cell lines

Human clear cell carcinoma (CCC) ovarian cancer cell lines (OVISE, OVTOKO, OVMANA and RMG-1) and serous adenocarcinoma (SAC) ovarian cancer cell lines (OVSAHO and OVKATE) were obtained from the Japanese Collection of Research Bioresources (JCRB, Osaka, Japan). Cells were maintained in RPMI 1640 medium supplemented with 10% fetal bovine serum (FBS) (HyClone Laboratories, Logan, UT) and 1% penicillin–streptomycin (Nacalai Tesque, Kyoto, Japan) at 37°C under a humidified atmosphere of 5% CO_2.

Protein extraction and 2D-DIGE

Proteins extracts of the cell lines were prepared with the Complete Mammalian Proteome Extraction Kit (Calbiochem, La Jolla, CA) and stored at −80°C until use. Protein concentrations were determined with the RC-DC Protein Assay kit (Bio-Rad Laboratories, Hercules, CA) using BSA as the standard. Before 2D-DIGE, we performed fluorescence labeling, for which the OVISE and OVSAHO samples were labeled with Cy3 and Cy5 CyDye DIGE fluorminimal dyes (GE Healthcare Bio-Sciences, Little Chalfont, Buckinghamshire, UK), respectively. For first-dimension separation, isoelectric focusing electrophoresis was performed using ReadyStrip™ (Bio-Rad Laboratories) IPG strips (24 cm, pH3-10NL). The labeled proteins (150 μg) were then loaded onto a gel strip, which was rehydrated in the dark for 12 hr (99,000 Vh) with the labeled protein sample diluted to 430 μl with a rehydration buffer (7 M urea, 2 M thiourea, 4% CHAPS, 2 mM TBP, 0.0002% BPB, 1.0% Bio-lyte 3-10 and 1.2% destreak). After isoelectric focusing, proteins were reduced in an equilibration buffer (50 mM Tris-HCl containing 6 M urea, 20% v/v glycerol and 2% SDS, pH 8.8) containing 20 mg/ml DTT for 40 min followed by carbamidomethylation in the equilibration buffer containing 25 mg/ml iodoacetamide for 30 min in the dark. The second-dimension separation was performed on 10% polyacrylamide gels using the Ettan-Dalt-Six system (GE Healthcare Bio-Sciences) at a constant wattage of 100 W at 20°C for 3 hr. Gel electrophoresis was performed in the dark, and the gels were scanned with the Typhoon scanner (GE Healthcare Bio-Sciences).

Protein identification by mass spectrometry

2D-PAGE was performed in parallel with 2D-DIGE using OVISE and OVSAHO protein extracts without fluorescence labeling. Gels were stained using a Silver Stain MS Kit (WAKO Pure Chemical Industries, Ltd., Osaka, Japan). Protein spots in a silver-stained gel, corresponding to the spots of interest in the 2D-DIGE scanned image, were digested in gel according to a previously described method,[16] using sequencing grade modified trypsin (Promega, Inc., Madison, WI). Digested peptides were then extracted with 5% TFA in acetonitrile (ACN/DW 50:45), sonicated for 5 min and concentrated by evaporation. The peptides were solubilized with 0.1% TFA in ACN/DW (2:98) and analyzed by means of LC-MS/MS. For reverse-phase separations, a Magic 2002 capillary HPLC (Michrom BioResources, Auburn, CA) with a C-18 RP column (length 15 cm, i.d. 200 μm; GL Sciences Inc., Tokyo, Japan) was used. The injected peptides were then eluted with a 30-min linear gradient of 5–65% of solvent B (solvent A: 0.1% formic acid in ACN/DW, 2:98; solvent B: 0.1% formic acid in ACN/DW, 95:5). The column was directly interfaced to an LCQ ion trap mass spectrometer (ThermoElectron, San Jose, CA) equipped with a nanoelectrospray ion source, and data were collected in the double mode that was configured to alternate between a single full MS scan and an MS/MS scan of the most intense precursor masses. MS/MS spectra were searched against the human protein Swiss-Prot database with the aid of the MASCOT search program (version 2.1.03; Matrix Science K.K., Tokyo, Japan). The following parameters were used for the search: enzyme: trypsin, missed cleavage; 1, variable modification; oxidation of methionines, fixed modification; carbamidomethylation of cysteins and monoisotopic peptide masses.

Real-time RT-PCR

For the quantification of Anx A4 mRNA in different ovarian cancer cell lines (CCC and SAC), we performed real-time RT-PCR. Total RNA was prepared from OVISE, OVTOKO, OVMANA, RMG-1 (CCC), OVSAHO and OVKATE (SAC) cell lines using an RNeasy Kit (Qiagen Valencia, CA) and cDNA was synthesized with a SuperScript™ III Reverse Transcriptase Kit (Invitrogen, Carlsbad, CA). A standard curve for Anx A4 cDNA was generated by the serial dilution of plasmid vector DNA, which encodes the Anx A4 gene. The primer sequences for Anx A4 were as follows: forward primer, 5′-ggaggtactgtcaaagctgc-3′ and reverse primer, 5′-gccactcagttctgacttcag-3′. Primers and cDNA were added to SYBR green premix (Invitrogen), which contained all the reagents required for PCR. The PCR conditions consisted of 1 cycle at 95°C for 1 min and 42 cycles of 95°C for 20 sec, 50°C for 20 sec and 72°C for 30 sec. PCR products were measured continuously with the My IQ™ Single-Color Real-Time Detection System (Bio-Rad Laboratories).

Western blotting

Cells and frozen tumor tissue samples were lysed in RIPA buffer (10 mM Tris-HCl, pH 7.5, 150 mM NaCl, 1% Nonidet P-40, 0.1% sodium deoxycholate, 0.1% SDS, 1 mM Na_3VO_4 and 1 × protease inhibitor cocktail (Nakalai Tesque)) followed by centrifugation (13,200 rpm, 4°C, 15 min), after which the supernatants were stored at −80°C until use. Protein concentrations were determined with the DC Protein Assay kit (Bio-Rad Laboratories), using BSA as the concentration standard. Extracted proteins were then resolved using 10% Bis-Tris Criterion XT Precast gels (Bio-Rad Laboratories) and subsequently transferred to PVDF membranes (Millipore, Bedford, MA). The membranes were washed and blocked with 1% skim milk in PBS containing 0.1% Tween 20 (PBST) and incubated with a goat polyclonal anti-Anx A4 antibody (sc-1930; Santa Cruz Biotechnology, Santa Cruz, CA) at a 1:300 dilution. Next, the membranes were incubated with horseradish peroxidase-conjugated donkey anti-goat IgG (Santa Cruz Biotechnology). Finally, the signals were visualized by means of an enhanced chemiluminescence (ECL) reaction system (Perkin-Elmer Life Sciences, Boston, MA). For loading control, western blotting and the subsequent antigen–antibody reaction were performed with GAPDH (Santa Cruz Biotechnology).

Immunohistochemistry

Expression of Anx A4 protein in ovarian cancer patient tissue sections was immunohistochemically measured with the ABC Kit (Vector Laboratories, Burlingame, CA). The total number of tissue section samples analyzed was 126 (43 CCC, 13 endometrioid, 8 mucinous, 62 SAC). Sections (3 μm) were prepared from formalin-fixed, paraffin-embedded tissue specimens, deparaffinized and rehydrated in graded alcohols. For antigen retrieval, the sections were incubated in a target retrieval solution (DAKO, Kyoto,